ALPHA RHYTHM SUBHARMONICS UNDERLIE RESPONSIVENESS TO THETA BURST STIMULATION VIA CALCIUM METAPLASTICITY

Kevin Kadak[1,2], Davide Momi[3], Zheng Wang[1], Sorenza P. Bastiaens[1,2], Mohammad P. Oveisi[1,4], Taha Morshedzadeh[1,2], Minarose Ismail[1,5], Jan Fousek[6], and John D. Griffiths[1,2,7]

[1]Krembil Centre for Neuroinformatics, Centre for Addiction and Mental Health, Toronto.

[2]Institute of Medical Sciences, University of Toronto

[3]Brain Stimulation Lab, Stanford Psychiatry and Behavioral Science, Stanford University

[4]Institute of Biomaterials and Biomedical Engineering, University of Toronto

[5]Department of Physiology, University of Toronto

[6]Central European Institute of Technology, Czech Republic

[7]Department of Psychiatry, University of Toronto

[*]*Corresponding author* – Email: kevin.e.kadak@gmail.com; john.griffiths@utoronto.ca;

August 28, 2025

Abstract

Repetitive transcranial magnetic stimulation (rTMS) is a non-invasive technique to modulate brain activity, often used in treating Major Depressive Disorder (MDD) by targeting fronto-limbic circuitry. Despite its clinical utility, optimizing rTMS protocols remains challenging due to the complex and variable effects of stimulation parameter changes on synaptic plasticity. Oscillatory brain activity, measurable via Electroencephalography (EEG), serves as a biomarker for functional circuits and treatment response. To better understand the impact of rTMS on brain oscillations and connectivity, we used computational modeling of corticothalamic circuits to explore the mechanisms of stimulus-induced plasticity. We integrated calcium-dependent plasticity (CaDP) with Bienenstock-Cooper-Munro (BCM) metaplasticity formulations in a neural population model of resting-state EEG. By varying protocol parameters, we simulated iTBS effects on spectral power, synaptic efficacy, and calcium concentrations. Our findings highlight a resonance between theta stimulation and individual resting-state alpha rhythms, enhancing incoming excitatory long-term depression (LTD) and inhibitory long-term potentiation (LTP), leading to corticothalamic feed-forward inhibition (FFI). Induced effects were encapsulated by a weakening of corticothalamic loops and enhancement of intrathalamic loops. This work offers a novel paradigm for individualizing iTBS treatments, provides insights into the neurophysiological basis of clinical responsiveness, and offers a framework with which to derive tailored protocols.

Introduction

Repetitive Transcranial magnetic stimulation (rTMS) is a non-invasive neuromodulatory tool for inducing functional changes in brain circuitry. As such, it is an effective treatment intervention for several neuropsychiatric disorders [1–4], most notably major depressive disorder (MDD) [5–7]. rTMS-MDD treatments have been substantially refined by the superior efficiency and smaller dosages of intermittent theta-burst stimulation (iTBS) against conventional high-frequency protocols (HF-rTMS), which has highlighted the profound influence of pulse structure, pattern, and volume on induced plasticity effects via long-term potentiation (LTP) and depression (LTD) mechanisms [8–13]. However, basic and clinical iTBS studies continue to report a high degree of heterogeneity in outcomes. Here we present and biologically justify an individualized iTBS paradigm for enhancing plasticity effects using a computational model of resting-state activity and rTMS-induced plasticity.

Resting-state electroencephalography (EEG) measures provide valuable insights into the intrinsic function of large-scale brain circuitry, with alpha oscillations (8-13 Hz) being its dominant spectral signature, believed to arise from time-delayed interactions between cortical and thalamic neural populations [14–17]. The frequency of a person's unique alpha rhythm, or individual alpha frequency (IAF), is considered a stable neurophysiological trait and has been used for evaluating MDD status, responsiveness, and guiding treatments [15, 18–23]. Recent research has demonstrated the utility of IAF as a means of personalizing rTMS treatments to enhance plasticity effects and clinical outcomes [24]. It is postulated that aligning stimulation frequencies with the dominant rhythm of the targeted corticothalamic circuit (i.e. alpha) could engage resonance with its endogenous activity. This may induce stronger plasticity effects to regulate oscillatory dynamics and improve MDD symptoms with greater efficacy than IAF-agnostic protocols [25–29, 18, 30, 19, 23, 21]. As IAFs are variable between subjects [31], their alignment discrepancy with the canonical 10 Hz HF-rTMS frequency may capture a considerable portion of clinical and experimental response variance, and offer a physiological signature upon which to tailor treatments.

The 5 Hz patterned pulse structure of iTBS is an exact subharmonic of the 10 Hz high-frequency rTMS (HF-rTMS), offering a congruence between the two paradigms. We propose a novel premise that iTBS protocols may be designed to act upon the same underlying synchrony mechanism to predict and enhance plasticity effects, but instead via alignment with the IAF's first subharmonic ($\mathrm{IAF}_{sub}^{1^{st}}$). To our knowledge, no research has been conducted to examine iTBS-alpha subharmonic interactions. However, IAF-synchronized HF-rTMS studies have yielded generally promising findings in recent years. A flagship IAF-synchronized rTMS study demonstrated significant sham-controlled improvements in MDD symptoms, with a greater severity of the symptoms predicting stronger outcomes [26, 29, 32]. Further studies have shown and replicated findings that the degree of IAF-rTMS frequency alignment predicted significantly stronger MDD treatment outcomes [18, 19, 23]. Additionally, closed-loop stimulation studies have demonstrated increased neuromodulatory efficacy in phase-locked rTMS interventions targeting frontal IAF oscillations [30] and sensorimotor μ-rhythms [33–36]. In TRD patients, IAF phased-locked interventions significantly improved symptoms, but with

non-superior efficacy against unsynchronized treatments [37, 38]. Similarly, an earlier study applying rTMS at IAF +1 Hz led to significantly reduced MDD symptoms, although with non-superior efficacy as 10 Hz treatments [39].

Assessing the effects of resonance in any rTMS paradigm remains difficult to probe experimentally, particularly in subcortical brain regions. Computational modelling can address several limitations of empirical EEG measures, as well as challenges posed by the diverse array of rTMS effects. EEG activity may be described and studied mathematically using tractable low-dimensional models of neural population dynamics for isolated examinations of rTMS-induced effects *in silico* [40]. Neural population models are a powerful class of mathematical equations that approximate the activity and properties of neural ensembles with a conservative set of state variables. These models have successfully captured many characteristic brain states and phenomena, including – most relevant to our discussion – eyes-open resting-state EEG regimes [41, 42]. To investigate how rTMS alters neural circuitry underlying resting-state EEG activity, we conducted numerical simulations using a corticothalamic neural population model with calcium-dependent plasticity (CaDP). In this model, rTMS-induced fluctuations in intracellular calcium concentrations determine the direction, magnitude, and timing of plasticity effects[43–46]. These calcium volume changes are homeostatically mediated by a Bienenstock-Cooper-Munro (BCM) metaplastic sliding threshold scheme via n-methyl-d-aspartate receptor (NMDAR) conductances, which ensures that synaptic weights remain both modifiable and stable (Fig. 1) [47–54]. The interplay of these mechanisms accounts for a variety of empirically observed TMS plasticity phenomena, including bidirectionality over pulse dose and time (i.e. LTP to LTD, vice versa)[43, 55–58] depending on paradigm (iTBS vs. cTBS, 10Hz vs. 1Hz). Disentangling these processes may shed light on the high variability in rTMS clinical response rates [59, 60].

Earlier modelling of TBS-induced CaDP with BCM metaplasticity demonstrated that stimuli saturation dynamics and calcium fluctuations can capture the invertible plasticity effects seen empirically [43, 61]. In separate works, alpha resonance was shown to lead to enhanced plasticity effects, and it was speculated that IAF-rTMS may therefore be optimal for treatments [62, 63]. However, these prior works have been confined to cortico-centric representations of the brain and have omitted the role of subcortical structures where rTMS treatment effects are also known to translate [64–66]. The thalamus is an embedded neural structure heavily implicated in alpha rhythmogenesis [17] and a crucially casual hub of MDD pathophysiology that has been increasingly validated as an rTMS treatment target [67, 68, 64, 69, 70]. Abnormal resting-state functional connectivity between the thalamus and frontal cortical structures (i.e. clinical TMS targets) has also been used to distinguish MDD status and predict rTMS treatment success [71, 64]. As rTMS is understood to correct dysfunctional oscillatory synchrony arising from functional imbalances in MDD-implicated pathways (particularly corticothalamic circuitry; [69, 67, 72–74]), spectral modulation may therefore be used as a generalized measure of rTMS effectiveness and a potential brain-based biomarker of clinical responsiveness [75]. Therefore, it is vital to represent the downstream circuitry that engenders EEG activity, is directly implicated in MDD pathophysiology, and plausibly bears deep importance on the interplay between IAF and iTBS.

We investigated how different iTBS protocols affect corticothalamic resting-state power spectra, connection weights, and LTD-LTP calcium levels. Our goal was to understand the relationship between rTMS parameters, individual

brain properties (IAF), and resultant plasticity effects to better guide approaches for enhancing induced plasticity in resting-state EEG circuitry. Protocols were varied by pulses-per-burst and inter-burst frequency parameters, which have previously been explored experimentally under the same theorized plasticity mechanisms [55, 76, 77]. Multiple regression analyses (MLR) with a significance threshold of $p < .001$ were conducted to assess robust effects across distinct alpha frequencies, circuit connections, and loops.

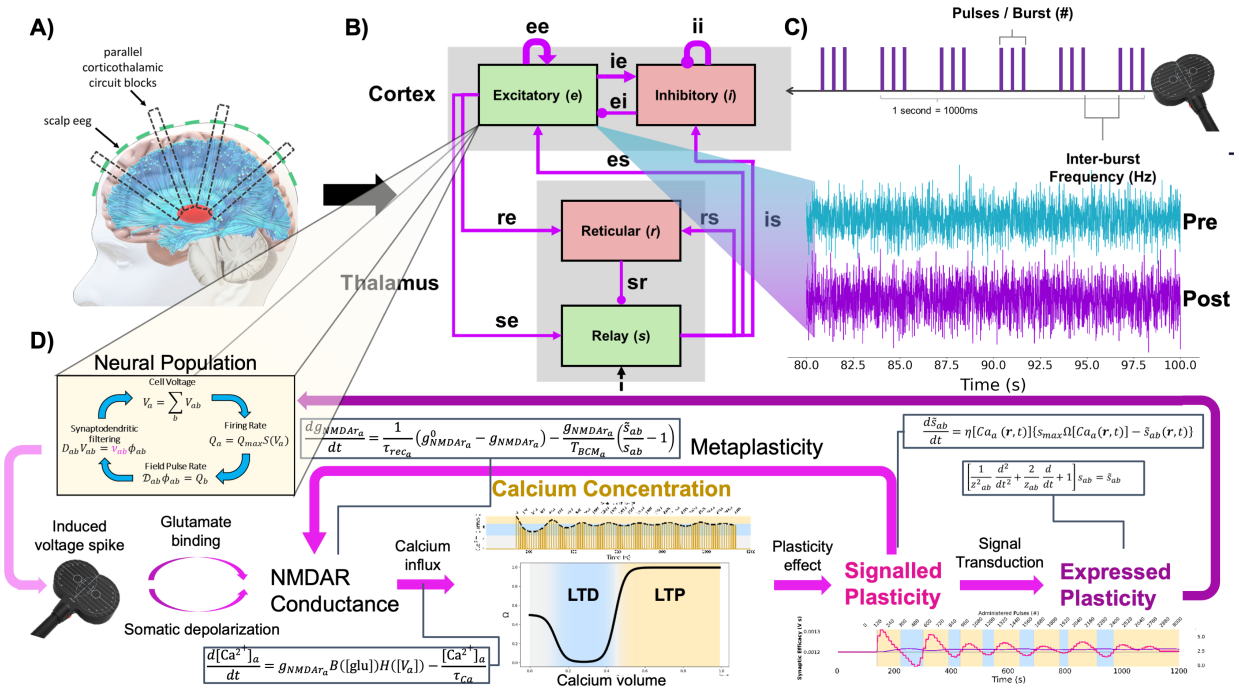

Figure 1: ***Examining iTBS-induced effects within a computational model of resting-state EEG activity integrated with calcium-dependent plasticity.*** Schematic of the methodology and neurophysiological model processes. **A)** Corticothalamic column underlying resting-state EEG activity and a **B)** 4-population corticothalamic neural population model of its circuitry, comprised of cortical excitatory pyramidal (e) and inhibitory interneuron (i) populations, and thalamic excitatory relay (s) and inhibitory reticular (r) nuclei populations. **C)** Intermittent theta-burst stimulation (iTBS) protocols deliver voltage-spiking stimuli to excitatory cortical populations. Cyan and purple timeseries depict pre- and post-stimulation resting-state activity, respectively, altered by plasticity-induced circuit modifications. **D)** Flowchart of Ca^{2+} scheme wherein post-synaptic depolarization and glutaminergic binding induce metaplastic NMDARs to open, enabling the influx of calcium to drive plasticity effects, with moderate and large concentrations driving LTD and LTP, respectively. Connection weight changes are immediately translated through signalled plasticity (a physiological analog of immediate, though functionally unrealized cell states) before manifesting as fully expressed functional modifications via altered ν values, following a signal transduction delay. In conjunction, NMDAR conductance is altered based on the prior weight dynamics, thereby mediating the next instance of calcium influx subsequent plasticity effect. The signaled ($\tilde{\nu}$; pink) and expressed (ν; purple) synaptic weight over pre, active, and post-canonical iTBS are shown for the excitatory-excitatory (ee) connection. Yellow and blue windows depict when modulated connection weight is relatively stronger and weaker than initial efficacy, respectively.

Results

iTBS induces resonant modulations to resting-state EEG spectra through alpha rhythm subharmonics

iTBS protocols induced a diverse array of modifications to corticothalamic circuitry, resulting in varying degrees of resting-state broadband power suppression. Power modulation scaled nonlinearly across the stimulation parameter values. Analyzing spectral power changes across stimulation parameter space revealed localized regions where the

strongest modulation occurred (Fig. 2A,C). These regions appear close to the natural frequency of the circuit (IAF; 10.5 Hz) and its first subharmonic ($\text{IAF}_{sub}^{1^{st}}$; 10.5 Hz / 2 = 5.25 Hz). This optimal frequency at the first subharmonic of alpha neighbored the 5 Hz carrier-wave ('theta') frequency of canonical iTBS. To confirm that these maximally-modulatory effects occurring in alignment with the alpha rhythm was indeed frequency-dependent, we ran a new set of simulations varying the dominant frequency of the circuit between 8-13 Hz (mimicking variable IAFs in humans) and examined the relative induced modulations. We observed a strong, significant positive correlation between the circuit's alpha frequency, its first subharmonic, and the inter-burst frequencies of maximally power-suppressing iTBS protocols. Changing the resting-state IAF by modifying the corticothalamic delay parameter t_0 (see section *Corticothalamic resting-state spectra and component measurement*) led to proportional shifts in the stimulation frequencies of maximally-modulating protocols, with the inter-burst frequency of the top modulatory protocols and circuit IAF being strongly correlated (r = .86, p < .001; Fig. 2C). The degree of broadband power suppression induced by canonical iTBS differed over resting-state frequencies, with the strongest modulation occurring at an alpha frequency of 9.5 Hz - wherein canonical iTBS was within 0.5 Hz of its first subharmonic (Fig. 2B, marked green). Consistent with this, we found a significant negative correlation (r = -.54, p < .001) between the simulated iTBS protocols' distance from the circuit's resting-state IAF and $\text{IAF}_{sub}^{1^{st}}$ - referred hereto as the alpha resonance distance (ARD) - and the degree of broadband power suppression. This negative correlation indicates that protocol-induced power modulation decreased as their inter-burst frequency became increasingly misaligned with the circuit's alpha frequency (Fig. 2D; top-left). MLR analyses confirmed that this anti-correlation between ARD and broadband power modulation persisted across different alpha frequencies, and was statistically significant across 9 of the 11 unique alpha frequencies following multiple comparison corrections (Table 1). Power modulation effects were also examined across pulses-per-burst, inter-burst frequency, and pulse rate protocol parameters. Significant negative and positive correlations with broadband power were observed, respectively, with the pulses-per-burst (r = -.54, p <.001) and inter-burst frequency (r = .44, p < .001) parameters, but not with pulse rate (r = -.131, p = .048; Fig. 2D). Heightened power modulation reflecting IAF-resonant engagement was visible along inter-burst frequency and pulse rate parameters.

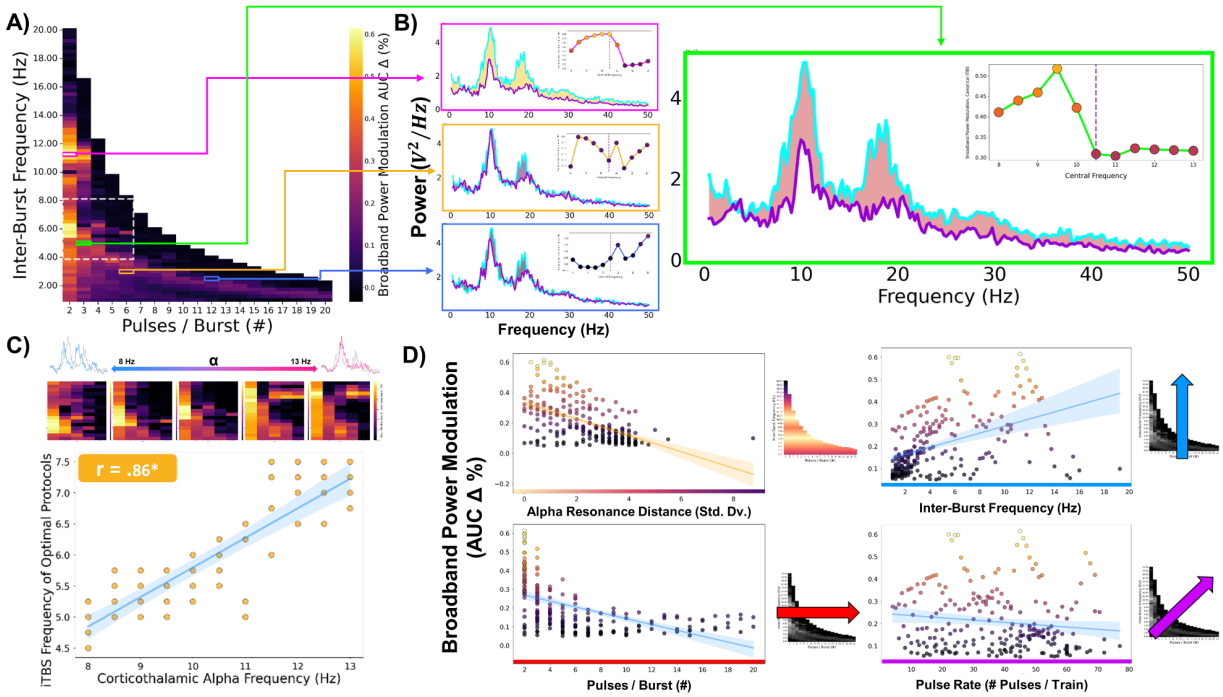

Figure 2: ***Induced broadband power modulation is enhanced by IAF-iTBS alignment.*** **A)** Heatmap of iTBS-induced broadband power suppression (pre - post AUC Δ) across parameter space (brighter = stronger suppression), with **B)** samples of power spectra prior to (cyan) and following (purple) stimulation, showing greater degrees of power modulation near alpha harmonic frequencies; green marks the canonical iTBS protocol. **C)** Further simulations with slowing/accelerating the alpha-band frequency show that IAF-iTBS resonance leads to proportional shifts in the inter-burst frequency of the most effective protocols. **D)** Broadband power change as a function of ARD (top-left), pulses-per-burst (bottom-left), inter-burst frequency (top-right), and pulse rate (bottom-right). Together these results support the premise that natural circuit frequency predicts the degree of iTBS-induced broadband power modulation.

Alpha-resonant iTBS protocols suppress broadband power by enhancing corticothalamic feed-forward inhibition

To better understand the circuit modifications responsible for engendering the broadband power modulations observed in our model, we next analyzed changes in plastic connection weights across the various stimulation parameters. This was done by examining both the directionality and absolute value of pre- vs. post-stimulation change in individual and circuit-mean connection weights (see Supplemental Fig. S1 for individual weight change heatmaps). As with the power modulations shown in Fig. 2, circuit-mean synaptic weight change showed a nonlinear, non-monotonic relationship with stimulation parameters (Fig.3A, C). Interestingly, we found that different iTBS protocols induced synaptic plasticity in unique ways to circuit connections, varying in both the number of affected connections and the magnitude of their modification. A sample of radar plot profiles shown in Fig. 3B demonstrate the unique weight change patterns induced by different protocols. A significant correlation between circuit-mean synaptic weight change was observed for inter-burst frequency ($r = -.31$, $p < .001$) and pulse rate (which showed a Gaussian distribution of modifications), but not for pulses-per-burst (Fig. 3C). ARD also showed no relationship with circuit-mean synaptic weight changes, indicating that IAF-iTBS resonance did not influence the degree of the cumulative plasticity effect. Notably, there was no robust relationship between circuit-mean synaptic weight change and broadband power modulation ($r = .196$, $p = .003$). There

was also considerable heteroscedasticity in the broadband power modulation values, with a progressively larger variance at higher levels of circuit-mean absolute synaptic weight change (3D). This result shows that circuit-wide synaptic weight modification alone is not a robust predictor of broadband power modulation, since large synaptic modifications can result in either low or high extents of power modulation. Next, we looked closer at individual connection weights within the circuit. We refer to connections whose values became larger relative to their pre-stimulation weight as *enhanced* (LTP; larger in magnitude and further from zero) and smaller as *dampened* (LTD; smaller in magnitude and closer to zero). MLR analyses showed significant relationships between synaptic weight change and broadband power modulation for several connections, with weight enhancements occurring within afferent connections to cortical inhibitory (i) and thalamic reticular (r) populations, and dampening within cortical excitatory (but not thalamic relay, s) populations. All inhibitory-afferent connections (i.e. inputs to inhibitory populations) demonstrated a significant interplay with ARD (Fig. 3E). However, only a subset of these connections were significantly modified as a function of ARD. Thalamic reticular-afferent connection weight change was negatively correlated with ARD, while cortical excitatory-afferent weight change was positively correlated, implying that ARD led to enhancement of thalamic reticular-afferent weights and dampening of cortical-afferent weights. These results are outlined in Table 2. This general phenomenon, whereby inhibitory activity is enhanced via excitatory inputs onto inhibitory neurons, is known as feed-forward inhibition (FFI). Thus, our results indicate that alpha-resonant iTBS protocols achieve broadband power suppression via selective modulation of corticothalamic FFI.

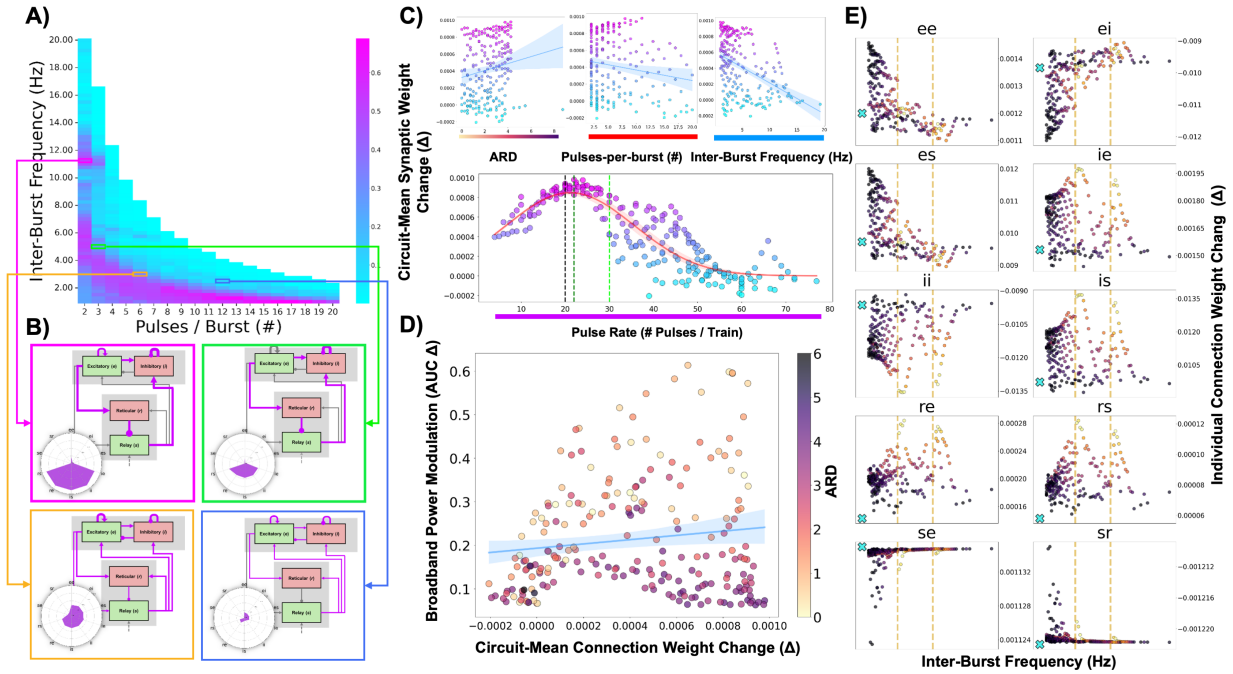

Figure 3: ***Selective synaptic modifications underlie broadband power modulation and demarcate protocol efficacy from circuit-wide plasticity effect.*** **A)** Heatmap of circuit-mean connection weight changes revealed a confined region of enhanced modification across parameter space distinct from broadband power suppression. **B)** Connection modification patterns for a sample of protocols illustrate unique synaptic plasticity effects from generalized circuit weight changes. **C)** Circuit-mean modifications adhere to a Gaussian distribution over protocol pulse rate, highlighting an optimal range within which plasticity is induced. Moreover, **D)** group-level weight modification and broadband power modulation are not statistically associated, implying a necessity to induce selective plasticity effects to compel functionally efficacious changes. **E)** Selective modifications are driven further by resonant effects, which visibly enhance inhibitory-afferent LTP across circuit connections.

Upregulation of feed-forward inhibition is corroborated by resonant engagement selectively facilitating and attenuating LTP-LTD calcium influx

Calcium release was induced during active iTBS across circuit connections, with different calcium volumes evoking different plasticity effects (LTD, LTP). As each plastic modulation altered NMDAR conductance rates, induced calcium volumes evolved non-monotonically over delivered pulses. To probe the low-level physiological drivers underpinning connection modifications across the circuit, and how they were influenced by rTMS pattern, we examined the relationship of LTD-LTP calcium volumes on broadband power and connection weight change, and as a product of ARD and pulse rate, the results of which are outlined in Table 3. Consistent with connection weight changes, LTP calcium volumes in circuit-wide inhibitory-afferent connections and LTD volumes in cortical excitatory-afferent connections were robustly associated with broadband power modulation. This implies that iTBS treatments drive FFI through calcium innervation, and IAF-resonance amplifies these influx patterns. Only circuit-mean LTP volumes, and not LTD volumes were significantly correlated with synaptic weight change ($r = .84$, $p < .001$) (Fig. 4E, F), implying that rTMS-induced LTP calcium was the principal driver of system change. Next, frequency interactions on calcium volumes were examined. MLR analyses were performed to compare ARD and induced LTD and LTP calcium volumes in each connection of the circuit. Thalamic relay-afferent connections se and sr were not included in these comparisons as

LTP calcium volumes were never induced within them. Interestingly, protocol ARD predicted systematically increased LTP calcium levels in thalamic inhibitory-afferent connections but attenuated levels in cortical excitatory-afferent connections, implying that resonant engagement facilitates influx for the former and blocks it for the latter. The opposite was true of LTD calcium, whose levels showed inverted trends with ARD, but were narrowly non-significant following multiple comparison corrections. Resonance-driven LTP calcium levels in thalamic rs connections and attenuated levels in cortical ei and es connections were statistically significant. Pulse rate was moderately and strongly anti-correlated with circuit-mean concentrations of LTD (r = -.36, p < .001) and LTP (r = -.85, p< .001), respectively, meaning that generalized calcium levels were attenuated in faster protocols (Fig. 4E, F).

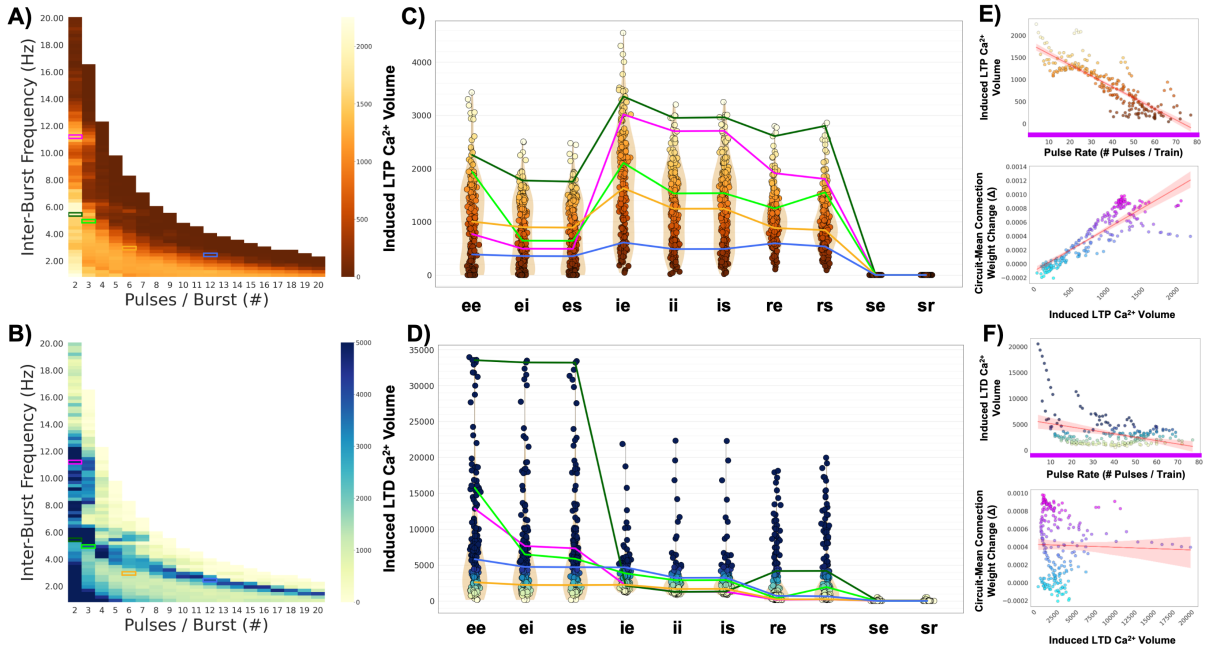

Figure 4: ***Induced calcium concentrations corroborate a two-pronged effect on spectra via inhibitory LTP and excitatory LTD.*** Heatmaps of circuit-mean **A)** LTP and **B)** LTD calcium volumes, as well as **C)** LTP and **D)** LTD volumes for each corticothalamic connection. Parameter changes induced unique patterns of calcium release, with protocol efficacy being defined by an amplification of LTP calcium globally and LTD calcium within cortical-excitatory afferent connections. These unique calcium effects are demonstrated across subset of different protocols, including standard (lime green) and model-optimal (dark green) iTBS. **E)** Circuit-mean LTP calcium volume decrease was strongly predicted by pulse rate increase and strongly predictive of circuit-mean connection weight change, while **F)** LTD volume decrease was only moderately predicted by pulse rate increase and not predictive of weight change.

Stimulation responsiveness is encapsulated by corticothalamic dampening and intrathalamic enhancement

To understand rTMS-induced effects on the circuit macroscopically, connection gains were computed (Eq. 14) and aggregated into the system's three major feedback loops (schematically depicted in Fig. 5A): Cortical (X), Corticothalamic (Y), and Intrathalamic (Z) (Eqs. 15, 16, 17). This enabled pre- and post-stimulation circuit states to be projected into the 3D XYZ loop gain space, which has been shown to capture all major dynamical regimes of the Robinson corticothalamic model [41, 78–82]. Our analyses showed that different iTBS protocols induced varying displacement in XYZ space from the initial pre-stimulation loop gains. These are shown in Fig. 5B, where each point

in the space corresponds to a post-stimulation loop gain configuration induced by a unique protocol. MLR analyses (Table 4) revealed a modest positive influence on broadband power modulation from X loop gains ($t = 4.18$, $p < .001$), a strong negative influence from Y loop gain ($t = -23.05$, $p < .001$), and a strong positive influence from Z loop gains ($t = 25.46$, $p < .001$) (Fig. 5C). Circuit modulation was thus strongly predicted by a protocol's propensity to dampen corticothalamic loop weights and enhance intrathalamic loop weights. A separate MLR analysis was performed to examine the resonance engagement of each loop gain. Significant resonant interactions occurred in cortiothalamic and intrathalamic loops, with ARD showing positive association with Y loop gains ($t = 5.74$, $p < .001$), negative association with Z loop gains ($t = -8.22$, $p < .001$), and no effect on X (cortical loop) gains (Fig. 5C, D). Modulatory resonance enhancements were also apparent across iTBS parameters in Y and Z, but not X loop gains (Supplemental Fig. S2).

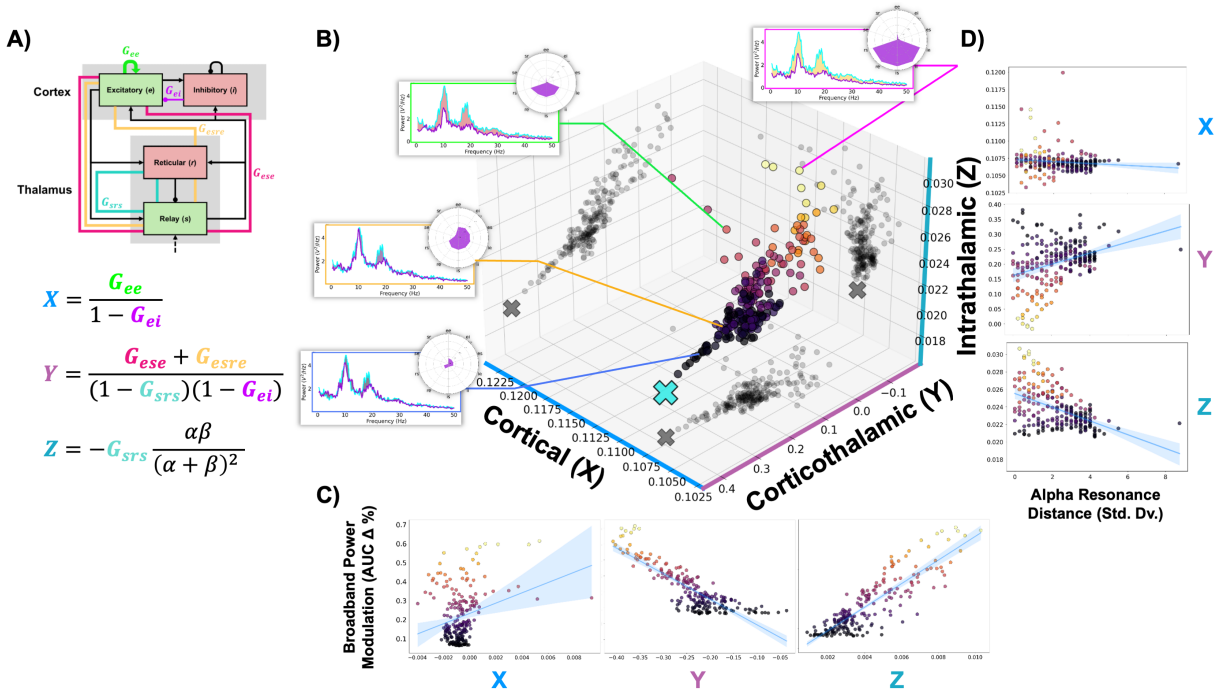

Figure 5: ***iTBS efficacy is robustly captured by corticothalamic dampening and intrathalamic enhancements of circuit loop gains.*** **A)** Corticothalamic connection gains may be mathematically collapsed into the circuit's three major loop gains: X (Cortical), Y (Corticothalamic), and Z (Intrathalamic). **B)** Post-stimulation circuit distributions in XYZ loop gain space show a robust trajectory in relation to broadband power change, with canonical (green) and a subset of novel iTBS protocols induce different displacements in space, corresponding to unique neurophysiological modifications. Point colors reflect broadband power modulation (as seen in Fig. 2A). **C)** Broadband power changes are shown to be a robust product of decreases and increases to Y and Z loop gains, respectively, implying downstream modifications bear the most functional importance on broadband power changes. These trends are further amplified by **D)** alpha resonance distance, which also manifests downstream to more strongly displace Y and Z circuit loop gains.

Discussion

We modeled and examined rTMS-induced plasticity effects on broadband power, synaptic weights, LTP/LTD calcium, and circuit loop gains within a corticothalamic neural mass model of resting-state EEG activity. We observed pattern-dependent modulation of these components, which were further amplified by a resonant interplay between IAF subharmonics and iTBS frequency. Here we outline the implications of these induced effects and outline the brain-stimulation mechanisms underlying them.

Mechanisms of action underlying iTBS protocol efficacy.

Previous empirical and modelling studies have examined stimulation effects across different amplitudes [83, 84, 59], pulse dosages [85–87], inter-train intervals [88, 89], treatment lengths [90, 91], session intervals [92], and other parameters against physiological and clinical outcomes. Here we extend this research by examining how stimulus pattern affects induced plasticity and their relationship to resting-state spectra. We propose that the dynamics observed in modelled parameter space, alongside empirically documented theta-burst effects, reflect the balanced engagement of four pattern-based mechanisms through which iTBS induces plasticity and drives robust responsiveness:

1. Endogenous theta mimicry: Theta oscillations are strongly implicated in active neural encoding processes, including learning and memory, and was the basis upon which the theta-burst stimulation protocol was originally formulated and adapted for human interventions [93, 94]. TBS mimics the frequencies associated with endogenous theta rhythms, which play a major role in plasticity phenomena in hippocampal tissue. This more effectively engages the mechanisms of NMDAR activation, calcium influx, and subsequent signaling cascades for LTD-LTP to achieve comparable plasticity effects as unpatterned rTMS with smaller pulse doses.

2. Intermittency: The intermittency of the iTBS pulse train structure allows for a larger calcium influx between recovery periods necessary for nominal LTP effects. This is in contrast to the continuous structure of cTBS which drives a consistent moderate calcium influx associated with LTD, in line with the principles of the calcium control hypothesis [44].

3. Pulse rate: Within the intermittent paradigm, the rate with which canonical iTBS delivers pulses lands within a range suitable for driving calcium innervation without oversaturating and downregulating the permeability of NMDARs mediating their plasticity effects, compelling more efficient and robust effects than protocols with smaller pulse intervals.

4. Circuit resonance: When delivered at a balanced intensity, the 5 Hz theta frequency of canonical iTBS enhances calcium innervation and subsequent LTP effects with greater efficacy when more closely aligned with the IAF (first subharmonic), which naturally varies between individuals.

Mechanisms 1 and 2 are well-established in literature [95, 96, 50, 93, 97], and our results strongly corroborate these proposed mechanisms of pulse rate (3) and circuit resonance (4) in several ways. Regarding pulse rate, we found an evident disadvantage for faster protocols, which venture away from the established theta-burst regime, have smaller

recovery periods, and increase the circuit's susceptibility to stimulation oversaturation compared to slower protocols, all of which attenuate LTP calcium - the driving force underlying efficacious circuit-wide modifications. Broadband power modulation was maximized in protocols with lower pulses-per-burst and inter-burst frequencies aligned with the first subharmonic, rather than the fundamental alpha (Fig. 2A). Pulse rate also had no predictive effect on broadband power change, implying no modulatory advantage for faster protocols (Fig. 2D). These effects were also present in fixed-amplitude conditions (Fig. S6). Notably, circuit-mean synaptic weight change was normally distributed across stimuli pulse rate, with the model-optimal protocol (2 pulses-per-burst, 5.50 Hz inter-burst frequency; 22 pulse rate) being congruent with the ideal pulse rate and neighboring that of HF-rTMS (20 pulse rate), as exemplified in Supplemental Fig. S4. Saturation effects were exemplified in fixed-amplitude protocol simulations, which showed that higher pulse rates strongly predicted increases in NMDAR modulation, thereby leading to metaplastic mechanisms being engaged and overall decreases in LTP calcium levels and broadband power modulation (see *Scaled vs. fixed metaplastic effects*). Finally, LTP calcium was strongly anti-correlated with pulse rate (Fig. 4E), suggesting that, even following amplitude-scaling, slower protocols compel the most favourable and robust modifications.

Our results also strongly emphasized the presence and modulatory enhancement of circuit resonance. We found robust relationships between protocol ARD and broadband power modulation (Fig. 2D), enhanced LTP calcium levels within thalamic reticular-afferent connections (Fig. 4A) and loop gains (Fig. 5D), and circuit-wide FFI. Resonant interactions were validated by proportional shifts in the efficacy of iTBS frequency across corticothalamic alpha frequencies (Fig. 2C). Protocol efficacy was characterized by enhanced LTP calcium in inhibitory-afferent projections and simultaneous LTD calcium in cortical excitatory-afferent projections. It was further revealed that ARD predicted an attenuation of opposing calcium concentrations in a subset of these connections, revealing an elegant two-pronged mechanism that drove and reinforced FFI (Fig. 4). This is especially notable given the diverse modification patterns observed across parameter space, and aligns with studies suggesting different iTBS protocols can uniquely affect cortical inhibition [98].

Anatomically speaking, the robust modulation of broadband spectral power observed in our model was driven by changes in corticothalamic and intrathalamic loops that lie downstream of the superficial cortical site where stimulation was applied. This finding is consistent with previous work showing that rTMS-TRD treatment success [67] is better predicted by stimulation-induced changes to fronto-thalamic, rather than frontal brain connections. Enhanced functional connectivity in corticothalamic circuits has also been identified as a core pathophysiological feature of MDD [71, 99], with symptom severity correlating with degree of hyperconnectivity [69]. Resonance manifesting in downstream corticothalamic and intrathalamic loop gains, but not in superficial cortical loop gains, corroborates the mechanism of action proposed by Leuchter and colleagues that IAF-rTMS may reset thalamocortical oscillations more effectively than frequency-agnostic protocols to correct aberrant functional configurations and drive clinical improvements [100, 28, 14, 27, 101, 18]. This resonance mechanism has clinical relevance given that heightened alpha power is a distinguishing EEG feature of MDD [102, 103, 20, 104, 105, 22], and its suppression has been linked to treatment responsiveness [106–109]. Studies have shown that individuals with more severe baseline symptoms of depression and anxiety showed enhanced responsiveness to alpha-synchronized rTMS [32, 29], suggesting that IAF-rTMS may

produce selective therapeutic effects for neuropsychiatric disorders characterized by abnormal resting-state patterns. Supplemental modelling analyses further revealed that alpha-band power suppression was strongly correlated with broadband power suppression and X and Y loop gain changes (Supplemental Fig. S3), supporting that rTMS also acts on alpha power via downstream circuit modifications. This is consistent with the dynamical regimes of the XYZ space as the distribution of induced loop gain weight changes captures a trajectory that departs from the alpha regime, leading to a reduction in power [42, 81].

We posit that iTBS leverages these four mechanisms over HF-rTMS to maximize nominal LTP effects and could explain why HF-rTMS treatments take longer to induce a comparable plasticity effect [110, 8]: A uniform, high-frequency pulse pattern and lack of an OFF period over-engage the homeostatic stability mechanisms described by BCM theory, leading to decreased NMDAR conductance despite administering pulses at similar rates. The clinical relevance of this mechanism is supported by empirical results showing that MDD patients have circuits with preferred resonant frequencies, and those with stronger resonance engagement at 10 Hz demonstrated both greater symptom severity at baseline and showed greater improvement with 10 Hz rTMS treatment than other slower or faster alpha frequencies [111]. Placebo-controlled 5 Hz rTMS has shown clinical effectiveness and non-inferior efficacy to 10 Hz treatments [112–119]. However, IAF has only been found to be predictive of improvement for 10 Hz treatments thus far [18]. This may be because 5 Hz rTMS uses only half the pulse rate of 10 Hz, suggesting that more stimuli are necessary to meaningfully engage circuitry before IAF-resonance becomes physiologically relevant. This suggests that resonance may be engaged via the IAF, but that protocols must remain within an optimal pulse rate range to qualify their induced effects, implicating both premises 3 and 4.

Individualized iTBS treatments, clinical applications, and takeaways.

Several methodological considerations warrant discussion. Our model assumes equality in the neuromodulatory capacity of each TMS pulse and LTD/LTP calcium thresholds across circuit connections, which may oversimplify the biological mechanisms underlying rTMS-induced plasticity effects. We address this by scaling TMS pulse amplitudes in our primary analyses emulate neural adaptation effects and isolate the contributions of stimulation pattern and saturation from protocol intensity. In addition, we assumed uniform LTD and LTP calcium thresholds across all circuit connections, which may be more accurately represented on an individual basis for calcium dynamics within each neural population or across circuits.

Whilst our primary findings (i.e. IAF resonance and low-intensity efficacy) and most of our results were consistent between scaled- and fixed-amplitude stimulation, some disparities still emerged, and these differences have implications for factors such as the choice of intensity ranges in physiological experiments. Thus, our approach enabled large-sweeping explorations of the rTMS parameter space that would not be possible without stimulation amplitude scaling, and future research should examine these assumptions in detail.

Key areas for future investigation include understanding the modulatory drop-off between fundamental and subharmonic alpha resonance, exploring individual power spectra components' interactions with iTBS, investigating spatial dynamics and stimulation targets [20, 120], and examining other temporal components such as intra-burst frequency [121]. Fitting individualized plasticity effect timescales, rather than using fixed values, could help explain response variability [43].

IAF-guided iTBS presents a promising approach for individualizing MDD treatments while requiring only minimal protocol modifications. Our results showed that resonant protocols targeting the first subharmonic of resting-state alpha induced the strongest modulation of resting-state spectra through excitatory-afferent LTD and inhibitory-afferent LTP calcium dynamics. These changes manifested in the dampening of corticothalamic loop gains and enhancement of intrathalamic gains.

Because alpha peak centrality is a robust and stable trait, patients' IAFs can be determined from a single resting-state EEG measure, even using low-cost mobile systems [15, 122]. We provide a neurophysiological basis for rTMS response and a computational framework for deriving individualized protocols. We hypothesize plasticity effects to undergo significantly greater modulation via IAF subharmonic resonance and encourage researchers to examine frequency alignment in iTBS datasets as a predictor variable, as our findings have important implications for understanding MDD mechanisms and improving treatment efficacy through personalized protocols.

Methods

The present work employed 4-population corticothalamic neural model, composed of excitatory pyramidal e and inhibitory interneuron i populations of the cortex, as well as excitatory relay s and inhibitory reticular r nuclei populations of the thalamus. Analyses examined relative changes in baseline synaptic weights and excitatory resting-state spectral power following 600 pulses of iTBS administered to the excitatory cortical population e. Primary analyses had all iTBS protocols administer pulses at an amplitude proportional to their stimulation intensity, and at a fixed amplitude (see *Stimulation intensity and protocol amplitude scaling*), delivered at a 50 Hz intra-burst frequency (20 ms pulse intervals) for 2 seconds ON, followed by 8 seconds OFF [95]. Stimulation protocols were varied across iTBS 'pulses-per-burst burst (#)' and 'inter-burst frequency (Hz)' parameter dimensions.

rTMS and iTBS have been shown to induce a diverse set of bidirectional spectral modulations across an array of frequency bins, and different protocol patterns may translate within unique components of the spectra [104, 123, 124]. Thus, to capture this range of effects, we examined broadband power modulation as the primary outcome and coefficient of rTMS-induced modification.

Neural population models

Neural population models are a set of mathematical equations that approximate the firing dynamics and physiological properties of neuronal populations to describe meso-macro scale activity in the brain. We refer the reader to [42] for a

holistic explanation. In a cyclical process, the mean somatic potential V_a of type a neurons are the result of summed afferent inputs from type b populations, captured as

$$V_a(t) = \sum_b V_{ab}(t) \tag{1}$$

where V_{ab} represents the post-synaptic potential of the recipient population a as a product of incoming inputs from population b at time t. Type b populations may represent an 'endogenous' population within the circuit (ie. e, i, r, or s) or an external stimulus input (ie. x; TMS). The synaptodendritic dynamics which mediate incoming inputs are described as

$$D_{ab}V_{ab}(t) = \nu_{ab}(t)\phi_{ab}(t - \tau_{ab}) \tag{2}$$

where coupling strength $\nu_{ab}(t)$ is the product of the mean synaptic weight s_{ab} multiplied by the mean number of synaptic connections N_{ab} between a and b populations (which we do not modify here). ϕ_{ab} is the mean axonal pulse rate from b to a and τ_{ab} is its signal propagation time delay between the populations; due to, for instance, the spatially extended pathways between cortical and thalamic populations. The operator D_{ab} describes the time evolution of V_{ab} in response to synaptic input, given by

$$D_{ab} = \left(\frac{1}{\alpha_{ab}}\frac{d}{dt} + 1\right)\left(\frac{1}{\beta_{ab}}\frac{d}{dt} + 1\right) \tag{3}$$

where α_{ab} and β_{ab} describe the inverse decay and rise response rates of the post-synaptic potentials, respectively. The resulting mean firing rate Q_a is related to mean somatic potential V_a through a sigmoidal function S_a, defined as

$$Q_a(t) = S_a[V_a(t)] = \frac{Q_a^{\max}}{1 + \exp\left[-\left\{V_a(t) - \theta_a\right\}/\sigma_a\right]} \tag{4}$$

where $Q_a^{\max}$ is the maximum possible firing rate, θ_a is the mean firing threshold, and σ_a is the standard deviation of the threshold. Finally, the firing of population a neurons generates axonal pulses which propagate along axons toward novel synapses of population c neurons. The mean axonal pulse rate is related to the mean firing rate by

$$\mathcal{D}_{ab}\phi_{ab}(t) = Q_b(t) \tag{5}$$

where

$$\mathcal{D}_{ab} = \left(\frac{1}{\gamma_{ab}}\frac{d}{dt} + 1\right)^2 \tag{6}$$

The parameter γ_{ab} represents the axonal propagation rate from neurons of type b to type a.

Calcium-dependent metaplasticity

We outline the approach of [40, 43] and reiterated by [61, 125] employed in the current work. A corticothalamic population model was outfitted with CaDP formulations incorporating a metaplastic Bienenstock-Cooper-Munro (BCM) sliding threshold scheme. Here, metaplasticity describes the dynamics of synaptic connections within the model whose weights ultimately change as a product of post-synaptic intracellular calcium (Ca^{2+}) volumes, which themselves are modulated by higher-order NMDAR calcium permeability rates (hence 'meta') [44, 45]. Synaptic weight values between an afferent a and efferent b population are plastic and dynamically modulated via the synaptodendtritic coupling strength term ν_{ab}, altered through its mean synaptic weight term s_{ab}, with expressed synaptic weight formulated as

$$\left(z_{ab}\frac{d}{dt}+1\right)^2 s_{ab} = \tilde{s}_{ab}. \tag{7}$$

Physiologically realized changes to synaptic weights are hypothesized to transpire following a protein cascade transduction from sporadic calcium-medicated plasticity processes. The given instance when connection weights are modified that eventually translate to measurable changes in synaptic efficacy, known as signaled synaptic strength $\tilde{s}_{ab}(t)$ and modelled as

$$\frac{d\tilde{s}_{ab}}{dt} = \eta([\mathrm{Ca}^{2+}]_a)(s_{max}\Omega([\mathrm{Ca}^{2+}]_a) - \tilde{s}_{ab}), \tag{8}$$

allows for non-monotonic changes in synaptic efficacy over time, leading to either functional LTP or LTD depending on the instance when stimulation is halted and modification concluded. As such, expressed synaptic weight acts as a low-pass filtered, homeostatically-stable translation of signalled synaptic weight change that will converge towards its modified end-value, with z_{ab} being the response timescale of the transduction delay between signalled and expressed plasticity. Put simply, signalled plasticity represents the immediate physiological synaptic efficacy state that is not yet functionally manifest while expressed plasticity represents the time-delayed, realized weight of the synapse that converges towards modified signalling. Post-synaptic calcium ion concentrations Ca^{2+} determine the directionality (LTP/D) and magnitude of induced plasticity at the point when stimulation is halted. Synaptic weight modification is driven by the calcium control functions of the plasticity rate

$$\eta = x\left([\mathrm{Ca}^{2+}]_a\right) + y\left([\mathrm{Ca}^{2+}]_a\right) \tag{9}$$

and the determinant plasticity effect induced

$$\Omega = \frac{x\left([\mathrm{Ca}^{2+}]_a\right)}{\eta\left([\mathrm{Ca}^{2+}]_a\right)}, \tag{10}$$

where low calcium concentrations lead to no meaningful plasticity effect, moderate concentrations induce LTD, and high concentrations induce LTP (to capture the BCM activation function). x and y are the calcium-dependent potentiation and depression rate functions, respectively, ascertained empirically from Shouval et al. [44, 45] (see [40] for the full expansion). Ca^{2+} is the product of pre-synaptic glutaminergic release and post-synaptic somatic depolarization, both of which are required for NMDARs to open and allow ionic influx, captured as

$$\frac{d[\mathrm{Ca}^{2+}]_a}{dt} = g_{NMDAr_a} B([\mathrm{glu}]) H(V) - \frac{[\mathrm{Ca}^{2+}]_a}{\tau_{[\mathrm{Ca}]}}. \tag{11}$$

g_{NMDAr} is the NMDAR conductance-mediated calcium permeability, B is the extent of NMDAR glutaminergic binding based on a sigmoid function of glutamate concentration $[\mathrm{glu}]$, H is the voltage-dependent threshold for NMDAR modulation (a nonlinear function which, increases with V, except for exceedingly strong depolarizations), and $\tau_{[\mathrm{Ca}]}$ is the timescale of calcium dynamics - the frequency with which calcium volumes update. Metaplasticity dynamics are integrated as a BCM sliding threshold scheme to describe adaptive changes in the g_{NMDAr} term, which would be otherwise fixed with base CaDP formulations (as seen in [40]). Here, the NMDAR conductance g_{NMDAr} that regulates post-synaptic Ca^{2+} influx rates and delineates LTD-LTP induction is moderated on the prior states of synaptic efficacy s_{ab}.

$$\frac{dg_{NMDAr_a}}{dt} = \frac{1}{\tau_{\mathrm{rec}_a}} \left(g^0_{NMDAr_a} - g_{NMDAr_a} \right) - \frac{g^0_{NMDAr_a}}{\tau_{\mathrm{BCM}_a}} \left(\frac{\tilde{s}_{ab}}{s_{ab}} - 1 \right) \tag{12}$$

where g^0_{NMDAr} is the calcium conductance at stability, s_{ab} is the expressed synaptic weight, and $\tilde{s}_{ab}$ is the projected synaptic weight towards which it trends. τ_{BCM} and τ_{rec} are the timescales for metaplasticity dynamics and calcium conductance to recover to the stable value, respectively. Post-synaptic glutamate concentrations $[\mathrm{glu}]$ are a product of pre-synaptic activity, which decay over a timescale $\tau_{[\mathrm{glu}]}$, modeled as

$$\frac{d[\mathrm{glu}]}{dt} = \lambda_{[\mathrm{glu}]} \phi_{ab} - \frac{[\mathrm{glu}]}{\tau_{[\mathrm{glu}]}} \tag{13}$$

where $\lambda_{[\mathrm{glu}]}$ is the mean glutamate concentration released per incoming pre-synaptic excitatory spike, ϕ_{ab} is the incoming pre-synaptic flux from excitatory populations, and $\tau_{[\mathrm{glu}]}$ is the timescale of glutamate decay.

Corticothalamic loop gains and space

Prior gain calculations by Robinson et al. have used the steady-state $\bar{\phi}$ to compute gains. However, because system states are continuously undergoing plasticity-induced changes throughout simulations, here we calculate the gain values at each time step. Altered system states are then ascertained by computing mean gain values from the final 10 seconds of simulated activity.

$$G_{ab} = \nu \frac{Q_{max}(\exp(-(V-\theta)/\sigma)}{\sigma(1+\exp(-(V-\theta)/\sigma))^2} \tag{14}$$

The individual gains for each connection can be reduced into 3 aggregate loop gains that capture the three major loops of the corticothalamic circuit: Cortical (X), Corticothalamic (Y), and Intrathalamic (Z), computed as

$$X = \frac{G_{ee}}{(1-G_{ei})} \tag{15}$$

$$Y = \frac{G_{ese}+G_{esre}}{(1-G_{srs})(1-G_{ei})} \tag{16}$$

$$Z = -G_{srs}\frac{\alpha\beta}{(\alpha+\beta)^2} \tag{17}$$

Model parameters and settings

All model-simulated outputs were generated with a step size (dt) of $\frac{1}{10{,}000}$ s and a write interval of $\frac{1}{1{,}000}$ s.

Corticothalamic state parameters were taken from from the NFTsim .conf library [126], outlined in Table 5. Initial ee and ei weights were modified within 20% of default value range to maintain circuit stability during and following stimulation, and to retain the oscillating evolution of plasticity signalling in excitatory-excitatory (ee) connections over pulses for canonical iTBS, as demonstrated in prior modelling [43].

Corticothalamic resting-state spectra and component measurement

Resting-state power spectra were computed using Welch's method from the voltage V of the excitatory cortical population using 120 seconds of activity prior to (pre) and following (post) iTBS administration. This population was chosen for its representation of the primary activity captured by EEG. Post-stimulation resting-state activity segments were sampled an additional 100 seconds after iTBS concluded to mitigate residual instability from affecting oscillatory dynamics and to allow for time-delayed ν values to converge towards $\tilde{\nu}$ values - with 100 seconds being the discrepancy timescale between signalled and expressed plasticity. Broadband power was computed from the area-under-curve (AUC) of the pre- and post-stimulation resting-state spectra (.25-50 Hz bin range) using the NumPy trapz function, formulated as

$$\Delta_{\text{Broadband Power}} = \int_{0.25\text{ Hz}}^{50\text{ Hz}} (PSD_{\text{pre}}(f) - PSD_{\text{post}}(f)). \tag{18}$$

In addition, alpha peak frequency and power were captured using the FOOOF library ([127]). Shifting the circuit's resting-state alpha frequency between 8-13 Hz was achieved by modifying corticothalamic delay timescales (t_0) from a standard .0425 s (the time for a signal to unidirectionally propagate between cortical and thalamic tracts)

to between .055 - .030 s for slower and faster frequencies, respectively. This mechanism is well understood and discussed in [41]. Alpha power change was assessed as the same pre-post difference as broadband power change. Alpha resonance distance (ARD) was computed as the standard deviation of a protocol's inter-burst frequency from the circuit's resting-state natural and first subharmonic alpha frequency. Smaller values equate to a smaller discrepancy between stimulation-endogenous frequency alignment.

Measurement of synaptic weight change

Synaptic weight change ($\Delta\nu$) were computed as the difference between the absolute post- and pre-stimulation connections weights, where a positive value denotes functional enhancement (further from 0, relative to its initial weight; LTP) and a negative value denotes dampening (closer to 0, relative to its initial weight; LTD). Synaptic weight change was assessed across individual connections and as a circuit-mean coefficient.

Measurement of calcium volumes

Calcium influx was induced during active iTBS. Calcium volumes were computed as the number of instances wherein stimuli drove calcium concentrations within LTD (0.25 – 0.45 μmol) and LTP (> 0.45 μmol) threshold ranges [45, 44, 43].

Measurement of loop gain change

Akin to synaptic weight change, corticothalamic loop gain change (see section *Corticothalamic loop gains and space*) was computed as the difference between post and pre-stimulation gains, with positive values denoting functional enhancement and negative values denoting dampening.

Stimulation intensity and protocol amplitude scaling

Across the parameter space, protocols of greater pulses-per-burst and inter-burst frequencies innately deliver stimuli faster than protocols with smaller parameter values. It was hypothesized that iTBS-induced effects would scale linearly with stimulation intensity, such that protocols that administer greater pulse volumes per train would modulate synaptic weights and oscillatory power more strongly than those that administer fewer. To account for the scaling stimulation intensities across the parameter space, isolate the temporo-modulatory effects of pulse pattern from intensity, and nullify effects of neural adaptation for different stimulation patterns, protocol pulse amplitudes were scaled as a product of their pulse rate (the process of which is depicted in Fig. S5). First, the pulse amplitude of canonical iTBS was established by finding the value that induced a steady-state oscillation in ee synaptic weight signaling ($\tilde{\nu}$), as was first demonstrated in a single-population model by [43]. Once the value was determined, the pulse amplitudes of all other protocols were scaled by their relative intensity to canonical iTBS, such that protocols of lesser relative intensity were administered with greater amplitudes (capped at double the canonical amplitude) and protocols of greater relative intensity were

administered with smaller amplitudes, respectively, explicitly calculated as the number of pulses delivered within a single iTBS train:

$$\text{Stimulation Intensity} = \text{Pulses-per-burst} \times \text{Inter-Burst Frequency} \times \text{ON-Time} \tag{19}$$

the dot product of the number of pulses-per-burst and the inter-burst frequency, multiplied by the length (in seconds) of the 'active' train stimulation period (fixed at a standard 2-second ON). Protocols amplitudes were adjusted through this scaling to produce equivalent stimulation intensities. To further validate the observed effects, supplemental analyses also tested protocols with a fixed amplitude derived from the approach used to determine the canonical iTBS value (see *Supplementary materials*).

rTMS parameters

rTMS protocols were varied across pulses-per-burst (#) and inter-burst frequency (Hz) parameters. Of the 432 unique protocols, 219 were included for statistical analyses based on their capacity to modulate broadband power at or beyond 10% of the maximum power modulation induced. This was done to ensure a minimal threshold of induced modification was included and non-effect protocols did not confound statistical outcomes.

Statistical testing

A threshold of $p < .001$ was used to classify statistical significance. Bonferroni multiple comparison corrections were performed for multiple linear regression analyses of individual alpha frequencies, synaptic weights and calcium LTP and LTD concentrations for each connection, and circuit loop gains.

Computing

Data loading, processing, analysis, and visualization were computed using Python 3.8.6 on the Compute Canada: Niagara high-performance computing cluster (Digital Research Alliance of Canada) and the CAMH Specialized Computing Cluster (SCC). Neural mass model simulations were performed using the open-source NFTsim C++ package [126]. The codebase for simulating and analyzing this work may be found at: `https://github.com/GriffithsLab/Kadak2025_alpha-subharmonics-rtms-eeg`.

References

[1] Marcelo T Berlim, Nicholas H Neufeld, and Frederique Van den Eynde. Repetitive transcranial magnetic stimulation (rTMS) for obsessive–compulsive disorder (OCD): an exploratory meta-analysis of randomized and sham-controlled trials. *Journal of psychiatric research*, 47(8):999–1006, 2013.

[2] Aurelia Gay, Julien Cabe, Ingrid De Chazeron, Celine Lambert, Maxime Defour, Vikesh Bhoowabul, Thomas Charpeaud, Aurore Tremey, Pierre-Michel Llorca, Bruno Pereira, et al. Repetitive transcranial magnetic

stimulation (rTMS) as a promising treatment for craving in stimulant drugs and behavioral addiction: a meta-analysis. *Journal of Clinical Medicine*, 11(3):624, 2022.

[3] Jack JQ Zhang, Kenneth NK Fong, Rang-ge Ouyang, Andrew MH Siu, and Georg S Kranz. Effects of repetitive transcranial magnetic stimulation (rTMS) on craving and substance consumption in patients with substance dependence: a systematic review and meta-analysis. *Addiction*, 114(12):2137–2149, 2019.

[4] Mohamed Attia, David McCarthy, and Mowafak Abdelghani. Repetitive transcranial magnetic stimulation for treating chronic neuropathic pain: a systematic review. *Current pain and headache reports*, 25(7):48, 2021.

[5] John P O'Reardon, H Brent Solvason, Philip G Janicak, Shirlene Sampson, Keith E Isenberg, Ziad Nahas, William M McDonald, David Avery, Paul B Fitzgerald, Colleen Loo, et al. Efficacy and safety of transcranial magnetic stimulation in the acute treatment of major depression: a multisite randomized controlled trial. *Biological psychiatry*, 62(11):1208–1216, 2007.

[6] Jean-Philippe Miron, Véronique Desbeaumes Jodoin, Paul Lespérance, and Daniel M Blumberger. Repetitive transcranial magnetic stimulation for major depressive disorder: basic principles and future directions. *Therapeutic Advances in Psychopharmacology*, 11:20451253211042696, 2021.

[7] Simone Rossi, Andrea Antal, Sven Bestmann, Marom Bikson, Carmen Brewer, Jürgen Brockmöller, Linda L Carpenter, Massimo Cincotta, Robert Chen, Jeff D Daskalakis, et al. Safety and recommendations for tms use in healthy subjects and patient populations, with updates on training, ethical and regulatory issues: Expert guidelines. *Clinical Neurophysiology*, 132(1):269–306, 2021.

[8] Daniel M Blumberger, Fidel Vila-Rodriguez, Kevin E Thorpe, Kfir Feffer, Yoshihiro Noda, Peter Giacobbe, Yuliya Knyahnytska, Sidney H Kennedy, Raymond W Lam, Zafiris J Daskalakis, et al. Effectiveness of theta burst versus high-frequency repetitive transcranial magnetic stimulation in patients with depression (THREE-D): a randomised non-inferiority trial. *The Lancet*, 391(10131):1683–1692, 2018.

[9] Nathan Bakker, Saba Shahab, Peter Giacobbe, Daniel M Blumberger, Zafiris J Daskalakis, Sidney H Kennedy, and Jonathan Downar. rTMS of the dorsomedial prefrontal cortex for major depression: safety, tolerability, effectiveness, and outcome predictors for 10 Hz versus intermittent theta-burst stimulation. *Brain stimulation*, 8 (2):208–215, 2015.

[10] Simone Rossi, Mark Hallett, Paolo M Rossini, Alvaro Pascual-Leone, Safety of TMS Consensus Group, et al. Safety, ethical considerations, and application guidelines for the use of transcranial magnetic stimulation in clinical practice and research. *Clinical neurophysiology*, 120(12):2008–2039, 2009.

[11] Colleen K Loo, Tara F McFarquhar, and Philip B Mitchell. A review of the safety of repetitive transcranial magnetic stimulation as a clinical treatment for depression. *International Journal of Neuropsychopharmacology*, 11(1):131–147, 2008.

[12] Leo Chen, Sung Wook Chung, Kate E Hoy, and Paul B Fitzgerald. Is theta burst stimulation ready as a clinical treatment for depression? *Expert review of neurotherapeutics*, 19(11):1089–1102, 2019.

[13] Hartwig Siebner and John Rothwell. Transcranial magnetic stimulation: new insights into representational cortical plasticity. *Experimental brain research*, 148:1–16, 2003.

[14] András Kondacs and Mihály Szabó. Long-term intra-individual variability of the background EEG in normals. *Clinical Neurophysiology*, 110(10):1708–1716, 1999.

[15] Thomas H Grandy, Markus Werkle-Bergner, Christian Chicherio, Florian Schmiedek, Martin Lövdén, and Ulman Lindenberger. Peak individual alpha frequency qualifies as a stable neurophysiological trait marker in healthy younger and older adults. *Psychophysiology*, 50(6):570–582, 2013.

[16] Shanice EW Janssens, Alexander T Sack, Sanne Ten Oever, and Tom A de Graaf. Calibrating rhythmic stimulation parameters to individual electroencephalography markers: The consistency of individual alpha frequency in practical lab settings. *European Journal of Neuroscience*, 55(11-12):3418–3437, 2022.

[17] Sorenza P Bastiaens, Davide Momi, and John D Griffiths. A comprehensive investigation of intracortical and corticothalamic models of the alpha rhythm. *PLOS Computational Biology*, 21(4):e1012926, 2025.

[18] Juliana Corlier, Linda L Carpenter, Andrew C Wilson, Eric Tirrell, A Polly Gobin, Brian Kavanaugh, and Andrew F Leuchter. The relationship between individual alpha peak frequency and clinical outcome with repetitive transcranial magnetic stimulation (rTMS) treatment of major depressive disorder (MDD). *Brain stimulation*, 12(6):1572–1578, 2019.

[19] Charlotte L Roelofs, Noralie Krepel, Juliana Corlier, Linda L Carpenter, Paul B Fitzgerald, Zafiris J Daskalakis, Indira Tendolkar, Andrew Wilson, Jonathan Downar, Neil W Bailey, et al. Individual alpha frequency proximity associated with repetitive transcranial magnetic stimulation outcome: An independent replication study from the ICON-DB consortium. *Clinical Neurophysiology*, 132(2):643–649, 2021.

[20] Natalia Jaworska, Pierre Blier, Wendy Fusee, and Verner Knott. Alpha power, alpha asymmetry and anterior cingulate cortex activity in depressed males and females. *Journal of psychiatric research*, 46(11):1483–1491, 2012.

[21] Rachel Lian, Vy Nguyen, and Rustin Berlow. EEG individual alpha frequencies may predict clinical outcome in TMS treatment. *Brain Stimulation: Basic, Translational, and Clinical Research in Neuromodulation*, 16(4):13, 2023.

[22] Ezra E Smith, Craig E Tenke, Patricia J Deldin, Madhukar H Trivedi, Myrna M Weissman, Randy P Auerbach, Gerard E Bruder, Diego A Pizzagalli, and Jürgen Kayser. Frontal theta and posterior alpha in resting EEG: A critical examination of convergent and discriminant validity. *Psychophysiology*, 57(2):e13483, 2020.

[23] Helena TS Voetterl, Alexander T Sack, Sebastian Olbrich, Sven Stuiver, Renee Rouwhorst, Amourie Prentice, Diego A Pizzagalli, Nikita van der Vinne, Jeroen A van Waarde, Martin Brunovsky, et al. Alpha peak frequency-based Brainmarker-I as a method to stratify to pharmacotherapy and brain stimulation treatments in depression. *Nature Mental Health*, 1(12):1023–1032, 2023.

[24] Ali Jannati, Lindsay M Oberman, Alexander Rotenberg, and Alvaro Pascual-Leone. Assessing the mechanisms of brain plasticity by transcranial magnetic stimulation. *Neuropsychopharmacology*, 48(1):191–208, 2023.

[25] Wolfgang Klimesch, Paul Sauseng, and Christian Gerloff. Enhancing cognitive performance with repetitive transcranial magnetic stimulation at human individual alpha frequency. *European Journal of Neuroscience*, 17 (5):1129–1133, 2003.

[26] Yi Jin and Bill Phillips. A pilot study of the use of EEG-based synchronized transcranial magnetic stimulation (sTMS) for treatment of major depression. *BMC psychiatry*, 14:1–6, 2014.

[27] Andrew Francis Leuchter, Ian A Cook, Yi Jin, and Bill Phillips. The relationship between brain oscillatory activity and therapeutic effectiveness of transcranial magnetic stimulation in the treatment of major depressive disorder. *Frontiers in human neuroscience*, 7:39451, 2013.

[28] Giorgio Fuggetta and Nor Azila Noh. A neurophysiological insight into the potential link between transcranial magnetic stimulation, thalamocortical dysrhythmia and neuropsychiatric disorders. *Experimental neurology*, 245:87–95, 2013.

[29] Andrew F Leuchter, Ian A Cook, David Feifel, John W Goethe, Mustafa Husain, Linda L Carpenter, Michael E Thase, Andrew D Krystal, Noah S Philip, Mahendra T Bhati, et al. Efficacy and safety of low-field synchronized transcranial magnetic stimulation (sTMS) for treatment of major depression. *Brain stimulation*, 8(4):787–794, 2015.

[30] Brigitte Zrenner, Christoph Zrenner, Pedro Caldana Gordon, Paolo Belardinelli, Eric J McDermott, Surjo R Soekadar, Andreas J Fallgatter, Ulf Ziemann, and Florian Müller-Dahlhaus. Brain oscillation-synchronized stimulation of the left dorsolateral prefrontal cortex in depression using real-time EEG-triggered TMS. *Brain stimulation*, 13(1):197–205, 2020.

[31] Sarah L Garnaat, Andrew M Fukuda, Shiwen Yuan, and Linda L Carpenter. Identification of clinical features and biomarkers that may inform a personalized approach to rTMS for depression. *Personalized medicine in psychiatry*, 17:4–16, 2019.

[32] Noah S Philip, Andrew F Leuchter, Ian A Cook, Joe Massaro, John W Goethe, and Linda L Carpenter. Predictors of response to synchronized transcranial magnetic stimulation for major depressive disorder. *Depression and anxiety*, 36(3):278–285, 2019.

[33] Christoph Zrenner, Debora Desideri, Paolo Belardinelli, and Ulf Ziemann. Real-time EEG-defined excitability states determine efficacy of tms-induced plasticity in human motor cortex. *Brain stimulation*, 11(2):374–389, 2018.

[34] Christoph Zrenner, Paolo Belardinelli, Maria Ermolova, Pedro Caldana Gordon, Matti Stenroos, Brigitte Zrenner, and Ulf Ziemann. μ-rhythm phase from somatosensory but not motor cortex correlates with corticospinal excitability in EEG-triggered TMS. *Journal of neuroscience methods*, 379:109662, 2022.

[35] Christoph Zrenner, Gábor Kozák, Natalie Schaworonkow, Johanna Metsomaa, David Baur, David Vetter, Daniel M Blumberger, Ulf Ziemann, and Paolo Belardinelli. Corticospinal excitability is highest at the early rising phase of sensorimotor μ-rhythm. *NeuroImage*, 266:119805, 2023.

[36] Miles Wischnewski, Zachary J Haigh, Sina Shirinpour, Ivan Alekseichuk, and Alexander Opitz. The phase of sensorimotor mu and beta oscillations has the opposite effect on corticospinal excitability. *Brain stimulation*, 15 (5):1093–1100, 2022.

[37] Gregory W Price, Joseph WY Lee, Carrie-Anne L Garvey, and Nathan Gibson. The use of background EEG activity to determine stimulus timing as a means of improving rtms efficacy in the treatment of depression: a controlled comparison with standard techniques. *Brain stimulation*, 3(3):140–152, 2010.

[38] Mark S George, Sarah Huffman, Jayce Doose, Xiaoxiao Sun, Morgan Dancy, Josef Faller, Xingbao Li, Han Yuan, Robin I Goldman, Paul Sajda, et al. Eeg synchronized left prefrontal transcranial magnetic stimulation (TMS) for treatment resistant depression is feasible and produces an entrainment dependent clinical response: A randomized controlled double blind clinical trial. *Brain stimulation*, 16(6):1753–1763, 2023.

[39] Martijn Arns, Desirée Spronk, and Paul B Fitzgerald. Potential differential effects of 9 Hz rTMS and 10 Hz rTMS in the treatment of depression. *Brain Stimulation: Basic, Translational, and Clinical Research in Neuromodulation*, 3(2):124–126, 2010.

[40] PK Fung and PA Robinson. Neural field theory of calcium dependent plasticity with applications to transcranial magnetic stimulation. *Journal of theoretical biology*, 324:72–83, 2013.

[41] Peter A Robinson, Christopher J Rennie, James J Wright, H Bahramali, Evian Gordon, and Donald L Rowe. Prediction of electroencephalographic spectra from neurophysiology. *Physical Review E*, 63(2):021903, 2001.

[42] Peter A Robinson, Christopher J Rennie, Donald L Rowe, Susie C O'Connor, James J Wright, Evian Gordon, and Richard W Whitehouse. Neurophysical modeling of brain dynamics. *Neuropsychopharmacology*, 28(1): S74–S79, 2003.

[43] PK Fung and PA Robinson. Neural field theory of synaptic metaplasticity with applications to theta burst stimulation. *Journal of theoretical biology*, 340:164–176, 2014.

[44] Harel Z Shouval, Mark F Bear, and Leon N Cooper. A unified model of NMDA receptor-dependent bidirectional synaptic plasticity. *Proceedings of the National Academy of Sciences*, 99(16):10831–10836, 2002.

[45] Harel Z Shouval, Gastone C Castellani, Brian S Blais, Luk C Yeung, and Leon N Cooper. Converging evidence for a simplified biophysical model of synaptic plasticity. *Biological cybernetics*, 87(5):383–391, 2002.

[46] Makoto Nishiyama, Kyonsoo Hong, Katsuhiko Mikoshiba, Mu-Ming Poo, and Kunio Kato. Calcium stores regulate the polarity and input specificity of synaptic modification. *Nature*, 408(6812):584–588, 2000.

[47] Elie L Bienenstock, Leon N Cooper, and Paul W Munro. Theory for the development of neuron selectivity: orientation specificity and binocular interaction in visual cortex. *Journal of Neuroscience*, 2(1):32–48, 1982.

[48] Wickliffe C Abraham and Mark F Bear. Metaplasticity: the plasticity of synaptic plasticity. *Trends in neurosciences*, 19(4):126–130, 1996.

[49] Wickliffe C Abraham and Warren P Tate. Metaplasticity: a new vista across the field of synaptic plasticity. *Progress in neurobiology*, 52(4):303–323, 1997.

[50] Wickliffe C Abraham. Metaplasticity: tuning synapses and networks for plasticity. *Nature Reviews Neuroscience*, 9(5):387–387, 2008.

[51] Gina G Turrigiano and Sacha B Nelson. Homeostatic plasticity in the developing nervous system. *Nature reviews neuroscience*, 5(2):97–107, 2004.

[52] Robert S Zucker. Calcium-and activity-dependent synaptic plasticity. *Current opinion in neurobiology*, 9(3): 305–313, 1999.

[53] Gastone C Castellani, Elizabeth M Quinlan, Leon N Cooper, and Harel Z Shouval. A biophysical model of bidirectional synaptic plasticity: dependence on AMPA and NMDA receptors. *Proceedings of the National Academy of Sciences*, 98(22):12772–12777, 2001.

[54] Luk Chong Yeung, Harel Z Shouval, Brian S Blais, and Leon N Cooper. Synaptic homeostasis and input selectivity follow from a calcium-dependent plasticity model. *Proceedings of the National Academy of Sciences*, 101(41):14943–14948, 2004.

[55] Masashi Hamada, Yasuo Terao, Ritsuko Hanajima, Yuichiro Shirota, Setsu Nakatani-Enomoto, Toshiaki Furubayashi, Hideyuki Matsumoto, and Yoshikazu Ugawa. Bidirectional long-term motor cortical plasticity and metaplasticity induced by quadripulse transcranial magnetic stimulation. *The Journal of physiology*, 586(16): 3927–3947, 2008.

[56] Olga Lucía Gamboa, Andrea Antal, Vera Moliadze, and Walter Paulus. Simply longer is not better: reversal of theta burst after-effect with prolonged stimulation. *Experimental brain research*, 204:181–187, 2010.

[57] Masashi Hamada, Nagako Murase, Alkomiet Hasan, Michelle Balaratnam, and John C Rothwell. The role of interneuron networks in driving human motor cortical plasticity. *Cerebral cortex*, 23(7):1593–1605, 2013.

[58] Ying-Zu Huang, Ming-Kue Lu, Andrea Antal, Joseph Classen, Michael Nitsche, Ulf Ziemann, Michael Ridding, Masashi Hamada, Yoshikazu Ugawa, Shapour Jaberzadeh, et al. Plasticity induced by non-invasive transcranial brain stimulation: a position paper. *Clinical Neurophysiology*, 128(11):2318–2329, 2017.

[59] Paul B Fitzgerald, Kate E Hoy, Rodney J Anderson, and Zafiris J Daskalakis. A study of the pattern of response to rTMS treatment in depression. *Depression and anxiety*, 33(8):746–753, 2016.

[60] Virginia López-Alonso, Binith Cheeran, Dan Río-Rodríguez, and Miguel Fernández-del Olmo. Inter-individual variability in response to non-invasive brain stimulation paradigms. *Brain stimulation*, 7(3):372–380, 2014.

[61] Marcus T Wilson, Park K Fung, Peter A Robinson, Jonathan Shemmell, and John NJ Reynolds. Calcium dependent plasticity applied to repetitive transcranial magnetic stimulation with a neural field model. *Journal of computational neuroscience*, 41:107–125, 2016.

[62] PA Robinson. Neural field theory of synaptic plasticity. *Journal of Theoretical Biology*, 285(1):156–163, 2011.

[63] PK Fung, AL Haber, and PA Robinson. Neural field theory of plasticity in the cerebral cortex. *Journal of Theoretical Biology*, 318:44–57, 2013.

[64] Tim V Salomons, Katharine Dunlop, Sidney H Kennedy, Alastair Flint, Joseph Geraci, Peter Giacobbe, and Jonathan Downar. Resting-state cortico-thalamic-striatal connectivity predicts response to dorsomedial prefrontal rTMS in major depressive disorder. *Neuropsychopharmacology*, 39(2):488–498, 2014.

[65] Martin Tik, André Hoffmann, Ronald Sladky, Livia Tomova, Allan Hummer, Lucia Navarro de Lara, Henryk Bukowski, Jürgen Pripfl, Bharat Biswal, Claus Lamm, et al. Towards understanding rTMS mechanism of action: stimulation of the DLPFC causes network-specific increase in functional connectivity. *Neuroimage*, 162:289–296, 2017.

[66] Robin FH Cash, Anne Weigand, Andrew Zalesky, Shan H Siddiqi, Jonathan Downar, Paul B Fitzgerald, and Michael D Fox. Using brain imaging to improve spatial targeting of transcranial magnetic stimulation for depression. *Biological psychiatry*, 90(10):689–700, 2021.

[67] Cheng-Ta Li, Li-Fen Chen, Pei-Chi Tu, Shyh-Jen Wang, Mu-Hong Chen, Tung-Ping Su, and Jen-Chuen Hsieh. Impaired prefronto-thalamic functional connectivity as a key feature of treatment-resistant depression: a combined MEG, PET and rTMS study. *PLoS One*, 8(8):e70089, 2013.

[68] Basilis Zikopoulos and Helen Barbas. Pathways for emotions and attention converge on the thalamic reticular nucleus in primates. *Journal of Neuroscience*, 32(15):5338–5350, 2012.

[69] Elliot C Brown, Darren L Clark, Stefanie Hassel, Glenda MacQueen, and Rajamannar Ramasubbu. Thalamocortical connectivity in major depressive disorder. *Journal of affective disorders*, 217:125–131, 2017.

[70] Chengxiao Yang, Kunchen Xiao, Yujia Ao, Qian Cui, Xiujuan Jing, and Yifeng Wang. The thalamus is the causal hub of intervention in patients with major depressive disorder: Evidence from the granger causality analysis. *NeuroImage: Clinical*, 37:103295, 2023.

[71] Michael D Greicius, Benjamin H Flores, Vinod Menon, Gary H Glover, Hugh B Solvason, Heather Kenna, Allan L Reiss, and Alan F Schatzberg. Resting-state functional connectivity in major depression: abnormally increased contributions from subgenual cingulate cortex and thalamus. *Biological psychiatry*, 62(5):429–437, 2007.

[72] Qing-Mei Kong, Hong Qiao, Chao-Zhong Liu, Ping Zhang, Ke Li, Li Wang, Ji-Tao Li, Yun'Ai Su, Ke-Qing Li, Chao-Gan Yan, et al. Aberrant intrinsic functional connectivity in thalamo-cortical networks in major depressive disorder. *CNS neuroscience & therapeutics*, 24(11):1063–1072, 2018.

[73] Paul E Croarkin, Andrea J Levinson, and Zafiris J Daskalakis. Evidence for gabaergic inhibitory deficits in major depressive disorder. *Neuroscience & Biobehavioral Reviews*, 35(3):818–825, 2011.

[74] Kate EM Godfrey, Abby C Gardner, Sarah Kwon, William Chea, and Suresh D Muthukumaraswamy. Differences in excitatory and inhibitory neurotransmitter levels between depressed patients and healthy controls: a systematic review and meta-analysis. *Journal of psychiatric research*, 105:33–44, 2018.

[75] Brian Kobayashi, Ian A Cook, Aimee M Hunter, Michael J Minzenberg, David E Krantz, and Andrew F Leuchter. Can neurophysiologic measures serve as biomarkers for the efficacy of repetitive transcranial magnetic stimulation treatment of major depressive disorder? *International Review of Psychiatry*, 29(2):98–114, 2017.

[76] Masashi Hamada and Yoshikazu Ugawa. Quadripulse stimulation–a new patterned rTMS. *Restorative Neurology and Neuroscience*, 28(4):419–424, 2010.

[77] Nikolai H Jung, Bernhard Gleich, Norbert Gattinger, Catrina Hoess, Carolin Haug, Hartwig R Siebner, and Volker Mall. Quadri-pulse theta burst stimulation using ultra-high frequency bursts–a new protocol to induce changes in cortico-spinal excitability in human motor cortex. *PLoS One*, 11(12):e0168410, 2016.

[78] PA Robinson, CJ Rennie, and DL Rowe. Dynamics of large-scale brain activity in normal arousal states and epileptic seizures. *Physical Review E*, 65(4):041924, 2002.

[79] Peter A Robinson, CJ Rennie, Donald L Rowe, SC O'Connor, and E Gordon. Multiscale brain modelling. *Philosophical Transactions of the Royal Society B: Biological Sciences*, 360(1457):1043–1050, 2005.

[80] Frank Freyer, James A Roberts, Robert Becker, Peter A Robinson, Petra Ritter, and Michael Breakspear. Biophysical mechanisms of multistability in resting-state cortical rhythms. *Journal of Neuroscience*, 31(17): 6353–6361, 2011.

[81] RG Abeysuriya, CJ Rennie, and PA Robinson. Physiologically based arousal state estimation and dynamics. *Journal of Neuroscience Methods*, 253:55–69, 2015.

[82] RG Abeysuriya and PA Robinson. Real-time automated EEG tracking of brain states using neural field theory. *Journal of neuroscience methods*, 258:28–45, 2016.

[83] Paul B Fitzgerald, Sarah Fountain, and Zafiris J Daskalakis. A comprehensive review of the effects of rTMS on motor cortical excitability and inhibition. *Clinical neurophysiology*, 117(12):2584–2596, 2006.

[84] Frank Padberg, Peter Zwanzger, Martin E Keck, Norbert Kathmann, Patrick Mikhaiel, Robin Ella, Philipp Rupprecht, Heike Thoma, Harald Hampel, Nicola Toschi, et al. Repetitive transcranial magnetic stimulation (rTMS) in major depression: relation between efficacy and stimulation intensity. *Neuropsychopharmacology*, 27 (4):638–645, 2002.

[85] Charlotte Nettekoven, Lukas J Volz, Martha Kutscha, Eva-Maria Pool, Anne K Rehme, Simon B Eickhoff, Gereon R Fink, and Christian Grefkes. Dose-dependent effects of theta burst rTMS on cortical excitability and resting-state connectivity of the human motor system. *Journal of Neuroscience*, 34(20):6849–6859, 2014.

[86] Manon Desforges, Itay Hadas, Brian Mihov, Yan Morin, Mathilde Rochette Braün, Pantelis Lioumis, Reza Zomorrodi, Hugo Théoret, Martin Lepage, Zafiris J Daskalakis, et al. Dose-response of intermittent theta burst stimulation of the prefrontal cortex: A TMS-EEG study. *Clinical Neurophysiology*, 136:158–172, 2022.

[87] Daniel M McCalley, Daniel H Lench, Jade D Doolittle, Julia P Imperatore, Michaela Hoffman, and Colleen A Hanlon. Determining the optimal pulse number for theta burst induced change in cortical excitability. *Scientific reports*, 11(1):8726, 2021.

[88] Robin FH Cash, Aisha Dar, Jeanette Hui, Leo De Ruiter, Julianne Baarbé, Peter Fettes, Sarah Peters, Paul B Fitzgerald, Jonathan Downar, and Robert Chen. Influence of inter-train interval on the plastic effects of rTMS. *Brain Stimulation*, 10(3):630–636, 2017.

[89] Alexander Taghva, Robert Silvetz, Alex Ring, A Kim Keun-young, Kevin T Murphy, Charles Y Liu, and Yi Jin. Magnetic resonance therapy improves clinical phenotype and EEG alpha power in posttraumatic stress disorder. *Trauma Monthly*, 20(4), 2015.

[90] Daniel M Blumberger, Fidel Vila-Rodriguez, Wei Wang, Yuliya Knyahnytska, Michael Butterfield, Yoshihiro Noda, Shahak Yariv, Moshe Isserles, Daphne Voineskos, Nicholas J Ainsworth, et al. A randomized sham controlled comparison of once vs twice-daily intermittent theta burst stimulation in depression: A canadian rtms treatment and biomarker network in depression (CARTBIND) study. *Brain Stimulation*, 14(6):1447–1455, 2021.

[91] Mandana Modirrousta, Benjamin P Meek, and Sara L Wikstrom. Efficacy of twice-daily vs once-daily sessions of repetitive transcranial magnetic stimulation in the treatment of major depressive disorder: a retrospective study. *Neuropsychiatric disease and treatment*, pages 309–316, 2018.

[92] Fengyun Yu, Xinwei Tang, Ruiping Hu, Sijie Liang, Weining Wang, Shan Tian, Yi Wu, Ti-Fei Yuan, and Yulian Zhu. The after-effect of accelerated intermittent theta burst stimulation at different session intervals. *Frontiers in neuroscience*, 14:576, 2020.

[93] John Larson and Erin Munkácsy. Theta-burst LTP. *Brain research*, 1621:38–50, 2015.

[94] G Capocchi, M Zampolini, and J Larson. Theta burst stimulation is optimal for induction of LTP at both apical and basal dendritic synapses on hippocampal ca1 neurons. *Brain research*, 591(2):332–336, 1992.

[95] Ying-Zu Huang, Mark J Edwards, Elisabeth Rounis, Kailash P Bhatia, and John C Rothwell. Theta burst stimulation of the human motor cortex. *Neuron*, 45(2):201–206, 2005.

[96] Ying-Zu Huang, John C Rothwell, Rou-Shayn Chen, Chin-Song Lu, and Wen-Li Chuang. The theoretical model of theta burst form of repetitive transcranial magnetic stimulation. *Clinical Neurophysiology*, 122(5):1011–1018, 2011.

[97] Antonio Suppa, Y-Z Huang, K Funke, MC Ridding, B Cheeran, V Di Lazzaro, U Ziemann, and JC Rothwell. Ten years of theta burst stimulation in humans: established knowledge, unknowns and prospects. *Brain stimulation*, 9(3):323–335, 2016.

[98] Alia Benali, Jörn Trippe, Elke Weiler, Annika Mix, Elisabeth Petrasch-Parwez, Wolfgang Girzalsky, Ulf T Eysel, Ralf Erdmann, and Klaus Funke. Theta-burst transcranial magnetic stimulation alters cortical inhibition. *Journal of Neuroscience*, 31(4):1193–1203, 2011.

[99] Lijun Kang, Aixia Zhang, Ning Sun, Penghong Liu, Chunxia Yang, Gaizhi Li, Zhifen Liu, Yanfang Wang, and Kerang Zhang. Functional connectivity between the thalamus and the primary somatosensory cortex in major depressive disorder: a resting-state fmri study. *Bmc Psychiatry*, 18:1–8, 2018.

[100] T Paus, PK Sipila, and AP Strafella. Synchronization of neuronal activity in the human primary motor cortex by transcranial magnetic stimulation: an EEG study. *Journal of Neurophysiology*, 86(4):1983–1990, 2001.

[101] Andrew F Leuchter, Aimee M Hunter, David E Krantz, and Ian A Cook. Rhythms and blues: modulation of oscillatory synchrony and the mechanism of action of antidepressant treatments. *Annals of the New York Academy of Sciences*, 1344(1):78–91, 2015.

[102] Alexander S Korb, Ian A Cook, Aimee M Hunter, and Andrew F Leuchter. Brain electrical source differences between depressed subjects and healthy controls. *Brain topography*, 21:138–146, 2008.

[103] Vera A Grin-Yatsenko, Ineke Baas, Valery A Ponomarev, and Juri D Kropotov. Eeg power spectra at early stages of depressive disorders. *Journal of clinical neurophysiology*, 26(6):401–406, 2009.

[104] Aron T Hill, Itay Hadas, Reza Zomorrodi, Daphne Voineskos, Paul B Fitzgerald, Daniel M Blumberger, and Zafiris J Daskalakis. Characterizing cortical oscillatory responses in major depressive disorder before and after convulsive therapy: a TMS-EEG study. *Journal of affective disorders*, 287:78–88, 2021.

[105] Shalini Mahato and Sanchita Paul. Electroencephalogram (EEG) signal analysis for diagnosis of major depressive disorder (MDD): a review. *Nanoelectronics, Circuits and Communication Systems: Proceeding of NCCS 2017*, pages 323–335, 2019.

[106] John R Hughes and E Roy John. Conventional and quantitative electroencephalography in psychiatry. *The Journal of neuropsychiatry and clinical neurosciences*, 11(2):190–208, 1999.

[107] G Ulrich, E Renfordt, G Zeller, and K Frick. Interrelation between changes in the EEG and psychopathology under pharmacotherapy for endogenous depression. *Pharmacopsychiatry*, 17(06):178–183, 1984.

[108] Gia Han Le, Sabrina Wong, Sebastian Badulescu, Hezekiah Au, Joshua D Di Vincenzo, Hartej Gill, Lee Phan, Taeho Greg Rhee, Roger Ho, Kayla M Teopiz, et al. Spectral signatures of psilocybin, lysergic acid diethylamide (LSD) and ketamine in healthy volunteers and persons with major depressive disorder and treatment-resistant depression: A systematic review. *Journal of Affective Disorders*, 2024.

[109] Alexandre Guet-McCreight, Homeira Moradi Chameh, Frank Mazza, Thomas D Prevot, Taufik A Valiante, Etienne Sibille, and Etay Hay. In-silico testing of new pharmacology for restoring inhibition and human cortical function in depression. *Communications Biology*, 7(1):225, 2024.

[110] Vincenzo Di Lazzaro, Michele Dileone, Fabio Pilato, Fioravante Capone, Gabriella Musumeci, Federico Ranieri, Valerio Ricci, Pietro Bria, Riccardo Di Iorio, Chiara De Waure, et al. Modulation of motor cortex neuronal

networks by rtms: comparison of local and remote effects of six different protocols of stimulation. *Journal of neurophysiology*, 105(5):2150–2156, 2011.

[111] Andrew F Leuchter, Andrew C Wilson, Nikita Vince-Cruz, and Juliana Corlier. Novel method for identification of individualized resonant frequencies for treatment of major depressive disorder (MDD) using repetitive transcranial magnetic stimulation (rTMS): A proof-of-concept study. *Brain Stimulation*, 14(5):1373–1383, 2021.

[112] Mark S George, Ziad Nahas, Monica Molloy, Andrew M Speer, Nicholas C Oliver, Xing-Bao Li, George W Arana, S Craig Risch, and James C Ballenger. A controlled trial of daily left prefrontal cortex TMS for treating depression. *Biological psychiatry*, 48(10):962–970, 2000.

[113] Ziad Nahas, F Andrew Kozel, Xingbao Li, Berry Anderson, and Mark S George. Left prefrontal transcranial magnetic stimulation (TMS) treatment of depression in bipolar affective disorder: a pilot study of acute safety and efficacy. *Bipolar disorders*, 5(1):40–47, 2003.

[114] Demetrio Ortega Rumi, Wagner F Gattaz, Sergio Paulo Rigonatti, Moacyr Alexandro Rosa, Felipe Fregni, Marina Odebrecht Rosa, Carlos Mansur, Martin Luiz Myczkowski, Ricardo Alberto Moreno, and Marco Antonio Marcolin. Transcranial magnetic stimulation accelerates the antidepressant effect of amitriptyline in severe depression: a double-blind placebo-controlled study. *Biological psychiatry*, 57(2):162–166, 2005.

[115] Tung-Ping Su, Chih-Chia Huang, I-Hua Wei, et al. Add-on rtms for medication-resistant depression: a randomized, double-blind, sham-controlled trial in chinese patients. *Journal of Clinical Psychiatry*, 66(7): 930–937, 2005.

[116] Paul B Fitzgerald, Stephen Huntsman, Ranil Gunewardene, Jayashri Kulkarni, and Z Jeff Daskalakis. A randomized trial of low-frequency right-prefrontal-cortex transcranial magnetic stimulation as augmentation in treatment-resistant major depression. *International Journal of Neuropsychopharmacology*, 9(6):655–666, 2006.

[117] William J Triggs, Nikki Ricciuti, Herbert E Ward, Jing Cheng, Dawn Bowers, Wayne K Goodman, Benzi M Kluger, and Stephen E Nadeau. Right and left dorsolateral pre-frontal rTMS treatment of refractory depression: a randomized, sham-controlled trial. *Psychiatry research*, 178(3):467–474, 2010.

[118] Noah S Philip, S Louisa Carpenter, Samuel J Ridout, George Sanchez, Sarah E Albright, Audrey R Tyrka, Lawrence H Price, and Linda L Carpenter. 5 Hz repetitive transcranial magnetic stimulation to left prefrontal cortex for major depression. *Journal of Affective Disorders*, 186:13–17, 2015.

[119] Linda L Carpenter, Christine Conelea, Audrey R Tyrka, Emma S Welch, Benjamin D Greenberg, Lawrence H Price, Matthew Niedzwiecki, Agustin G Yip, Jennifer Barnes, and Noah S Philip. 5 hz repetitive transcranial magnetic stimulation for posttraumatic stress disorder comorbid with major depressive disorder. *Journal of Affective Disorders*, 235:414–420, 2018.

[120] Jonathan Downar and Z Jeff Daskalakis. New targets for rTMS in depression: a review of convergent evidence. *Brain stimulation*, 6(3):231–240, 2013.

[121] Steve W Wu, Nasrin Shahana, David A Huddleston, and Donald L Gilbert. Effects of 30 Hz theta burst transcranial magnetic stimulation on the primary motor cortex. *Journal of neuroscience methods*, 208(2): 161–164, 2012.

[122] Taha Morshedzadeh, Kevin Kadak, Sorenza P Bastiaens, M Parsa Oveisi1, Davide Momi1, Zheng Wang, Shreyas Harita, Maurice Abou Jaude, Christopher A Aimone, Steve Mann, et al. Corticothalamic modelling of sleep neurophysiology with applications to mobile eeg. *Sleep*, page zsaf086, 2025.

[123] Domenica Veniero, Alexandra Vossen, Joachim Gross, and Gregor Thut. Lasting EEG/MEG aftereffects of rhythmic transcranial brain stimulation: level of control over oscillatory network activity. *Frontiers in cellular neuroscience*, 9:477, 2015.

[124] Gregor Thut and Carlo Miniussi. New insights into rhythmic brain activity from TMS–EEG studies. *Trends in cognitive sciences*, 13(4):182–189, 2009.

[125] Marcus T Wilson, Bahar Moezzi, and Nigel C Rogasch. Modeling motor-evoked potentials from neural field simulations of transcranial magnetic stimulation. *Clinical Neurophysiology*, 132(2):412–428, 2021.

[126] Paula Sanz-Leon, Peter A Robinson, Stuart A Knock, Peter M Drysdale, Romesh G Abeysuriya, Felix K Fung, Chris J Rennie, and Xuelong Zhao. NFTsim: theory and simulation of multiscale neural field dynamics. *PLoS computational biology*, 14(8):e1006387, 2018.

[127] Thomas Donoghue, Matar Haller, Erik J Peterson, Paroma Varma, Priyadarshini Sebastian, Richard Gao, Torben Noto, Antonio H Lara, Joni D Wallis, Robert T Knight, et al. Parameterizing neural power spectra into periodic and aperiodic components. *Nature neuroscience*, 23(12):1655–1665, 2020.

Tables

Alpha Shifts

Alpha frequency (Hz)	$t_0/2$ (s)	ARD (IV)
13.0	.0300	**t = -7.42, p < .001**
12.5	.0305	**t = -7.20, p < .001**
12.0	.0310	**t = -5.01, p < .001**
11.5	.0320	**t = -4.11, p < .001**
11.0	.0360	t = -3.88, p < .001
10.5	.0425	**t = -10.01, p < .001**
10.0	.0460	**t = -6.18, p < .001**
9.5	.0470	**t = -5.98, p < .001**
9.0	.0480	**t = -5.45, p < .001**
8.5	.0490	**t = -4.47, p < .001**
8.0	.0550	t = -1.85, p = .711

Table 1: MLR coefficients between ARD and broadband power modulation over unique corticothalamic alpha frequencies. Bolded values represent statistical significance following multiple comparison corrections.

Synaptic Weight

Connection	Broadband power (DV)	ARD (IV)
ee	**t = -6.53, p < 0.001**	**t = 7.22, p < 0.001**
ei	**t = -6.23, p < 0.001**	**t = 6.93, p < 0.001**
es	**t = -6.17, p < 0.001**	**t = 6.90, p < 0.001**
ie	**t = 7.33, p < 0.001**	t = -0.55, p = 0.582
ii	**t = 9.16, p < 0.001**	t = -1.44, p = 0.151
is	**t = 9.15, p < 0.001**	t = -1.43, p = 0.154
re	**t = 25.63, p < 0.001**	**t = -5.81, p < 0.001**
rs	**t = 23.64, p < 0.001**	**t = -6.56, p < 0.001**
se	t = 2.59, p = 0.010	t = -2.70, p = 0.007
sr	t = 2.59, p = 0.010	t = -2.71, p = 0.007

Table 2: MLR coefficients for iTBS-induced modifications to corticothalamic connection weights ($\Delta\nu$), predictive of broadband power modulation and predicted by ARD. Bolded values represent statistical significance following multiple comparison corrections.

Calcium

	Broadband power (DV)		ARD (IV)	
Connection	**LTD**	**LTP**	**LTD**	**LTP**
ee	**t = 12.56, p < 0.001**	t = 2.85, p = 0.005	t = -3.38, p = 0.001	t = 3.32, p = 0.001
ei	**t = 10.73, p < 0.001**	t = 0.47, p = 0.636	-3.22, p = 0.001	**t = 4.68, p < 0.001**
es	**t = 10.64, p < 0.001**	t = 0.44, p = 0.660	-3.20, p = 0.002	**t = 4.70, p < 0.001**
ie	t = 0.58, p = 0.564	**t = 8.64, p < 0.001**	t = 1.54, p = 0.126	t = 0.01, p = 0.996
ii	t = 0.39, p = 0.693	**t = 9.69, p < 0.001**	t = 2.53, p = 0.012	t = -0.40, p = 0.689
is	t = 0.40, p = 0.689	**t = 9.69, p < 0.001**	t = 2.50, p = 0.013	t = -0.40, p = 0.687
re	t = 1.39, p = 0.167	**t = 17.42, p < 0.001**	t = 4.09, p < 0.001	t = -3.87, p < 0.001
rs	t = 1.57, p = 0.118	**t = 16.20, p < 0.001**	4.02, p < 0.001	**t = -5.75, p < 0.001**
se	t = -2.21, p = 0.028	N/A	2.15, p = 0.033	N/A
sr	t = -2.21, p = 0.028	N/A	2.15, p = 0.033	N/A

Table 3: MLR coefficients for induced LTD & LTP calcium volumes, predictive of broadband power modulation and predicted by ARD. Bolded values represent statistical significance following multiple comparison corrections.

Circuit loop gains

Loop	Broadband power (DV)	ARD (IV)
X	**t = 4.18, p < 0.001**	t = 2.02, p = 0.045
Y	**t = -23.05, p < 0.001**	**t = 5.74, p < 0.001**
Z	**t = 25.46, p < 0.001**	**t = -8.22, p < 0.001**

Table 4: MLR coefficients of corticothalamic loop gains change, predictive of broadband power modulation and predicted by ARD. Bolded values represent statistical significance following multiple comparison corrections.

Model parameters

Parameter	Value	Unit
Corticothalamic connection parameters		
ν_{ee}	0.001200	V s
ν_{ei}	-0.009839	V s
ν_{es}	0.009732	V s
ν_{ie}	0.001532	V s
ν_{ii}	-0.009639	V s
ν_{is}	0.009732	V s
ν_{re}	0.000143	V s
ν_{rs}	0.000058	V s
ν_{se}	0.001135	V s
ν_{sr}	-0.001222	V s
$t_0/2$	0.0425 (0.030-0.055)	s
Metaplasticity parameters		
θ_p	0.45	μM
θ_d	0.25	μM
z_{ab}	100	s
g_{NMDAr}	0.002	M $s^{-1}V^{-1}$
t_{BCM}	7	s
$t_{[\text{Ca}^{2+}]}$	0.05	s
t_{rec}	1000	s
$\tau_{[\text{Glu}]}$	0.003	s
$\lambda_{[\text{Glu}]}$	150e-6	μM s

Table 5: Corticothalamic neural population with metaplasticity model parameters.

Supplementary materials

Here we provide a set of additional content for rTMS-induced changes of individual synaptic weights and circuit loop gains, as well as alpha-band power changes and their relationship with said outcomes.

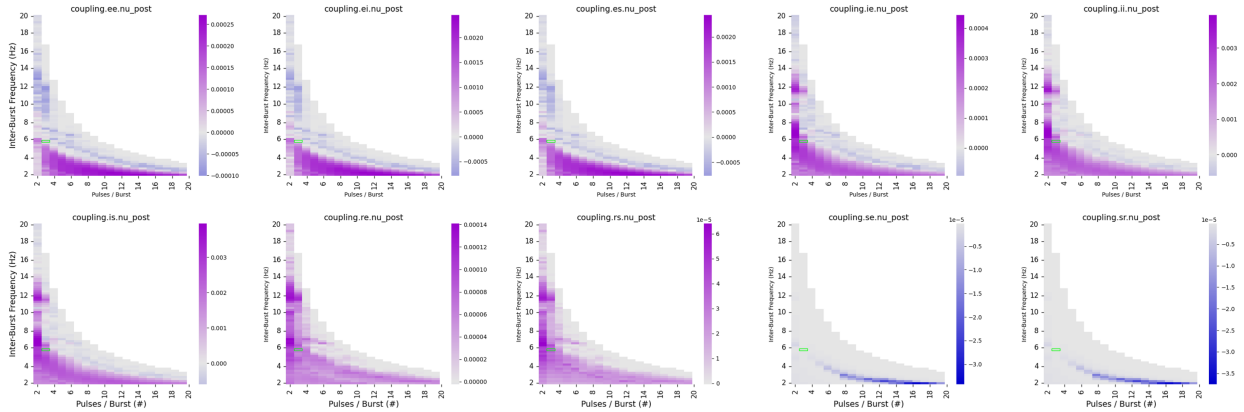

Figure S1: ***Heatmap of post-iTBS connection weights for each connection within the corticothalamic circuit. Purple denotes weight enhancements, while blue denotes reductions.***

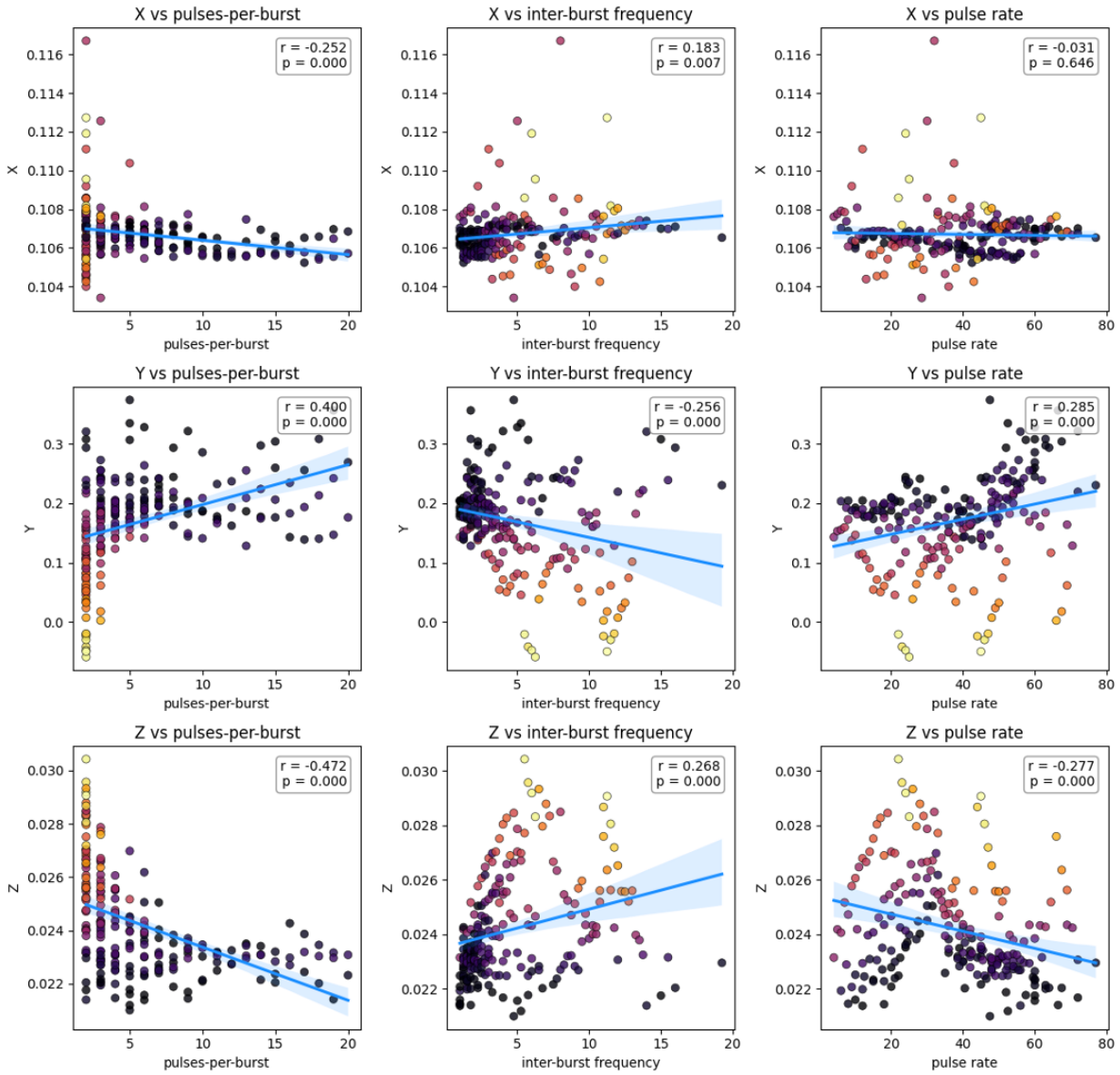

Figure S2: ***Scatterplot distributions of post-stimulation X, Y, and Z loop gains across pulses-per-burst, inter-burst frequency, and pulse rate iTBS parameters.***

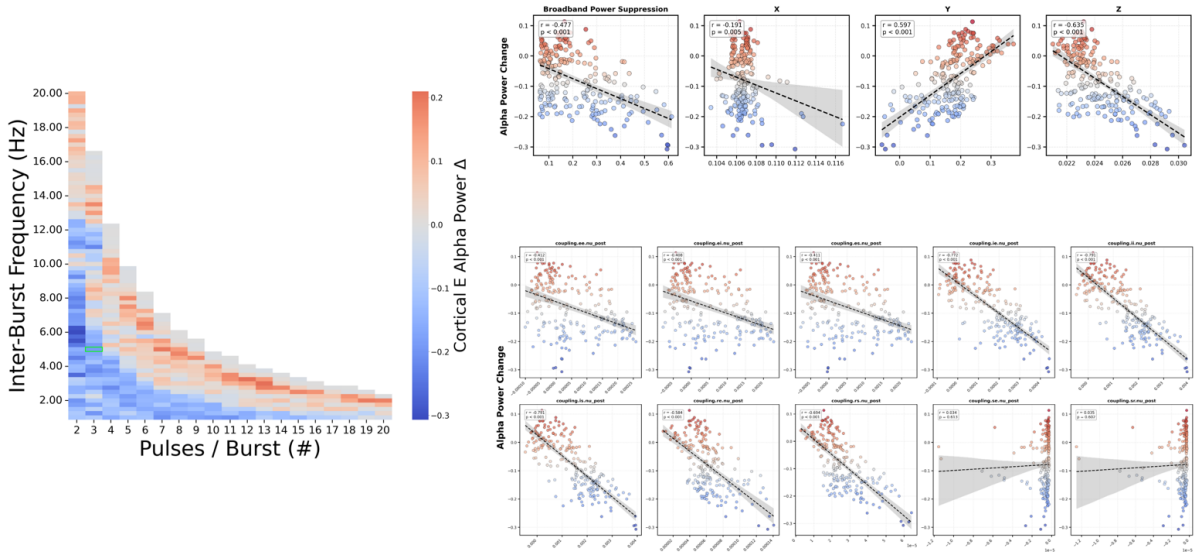

Figure S3: ***Relationship between iTBS-induced changes of alpha and broadband power, connection weights, and loop gains.***

Scaled vs. fixed metaplastic effects

We hypothesized that protocols that avoid oversaturating NMDAR conductance rates would drive a more consistent calcium influx and induce their effects more efficiently than those that cause fluctuations in conductance rates and subsequent calcium levels. We aimed to isolate the stimulation effects of pulse pattern and frequency from the byproduct of intensity by scaling pulse amplitudes in proportion to their administered rate, such that faster protocols had smaller amplitudes (see *Stimulation intensity and protocol amplitude scaling*). The results showed that the influence of protocol intensity on outcome measures was indeed removed, allowing us to focus on the patterned effects of stimuli. Only fixed-amplitude protocols demonstrated a robust significant relationship between pulse rate and engagement of circuit-mean metaplastic homeostasis (quantified as the standard deviation of NMDAR conductance rates during active iTBS). Additionally, metaplastic homeostasis was negatively related to broadband power modulation and plasticity-inducing calcium levels, and positively related to circuit-wide synaptic weight change. These effects were largely absent in scaled-amplitude protocols, with only circuit-mean connection weight change yielding a significant relationship NMDAR conductance rates (Supplemental Fig. S7). While the extent of connection weight change differed, the modification patterns associated with treatment efficacy were persistent between conditions. As depicted in the supplemental radar plots (Supplemental Fig. S6), there was a strong similarity in the relative synaptic modification patterns between scaled (purple) and fixed (green) simulations, validating that the induced effects are consistent between conditions.

These trends demarcate our scaled and fixed-amplitude conditions and confirm that our correction approach effectively 'detrended' the scaling energy contribution over pulse rate to isolate the influence of pulse pattern outcome measures. It

is important to note these NMDAR metaplasticity mechanisms were still very much engaged and functionally relevant in system dynamics and measured outcomes, but that the extent of their engagement was systematically corrected to enable more physiologically plausible and experimentally practical examinations of the parameter space. Our approach emphasizes that balancing pulse pattern and intensity, and understanding the role of metaplastic homeostasis mediating their effects, is crucial for formulating effective rTMS protocols.

We discern that protocols minimizing the engagement of metaplastic NMDAR homeostasis facilitate a more consistent calcium influx, leading to stronger and more efficient modulatory effects. Conversely, protocols that engage metaplastic homeostasis more aggressively tend to result in fluctuating calcium permeability and less efficient plasticity trends.

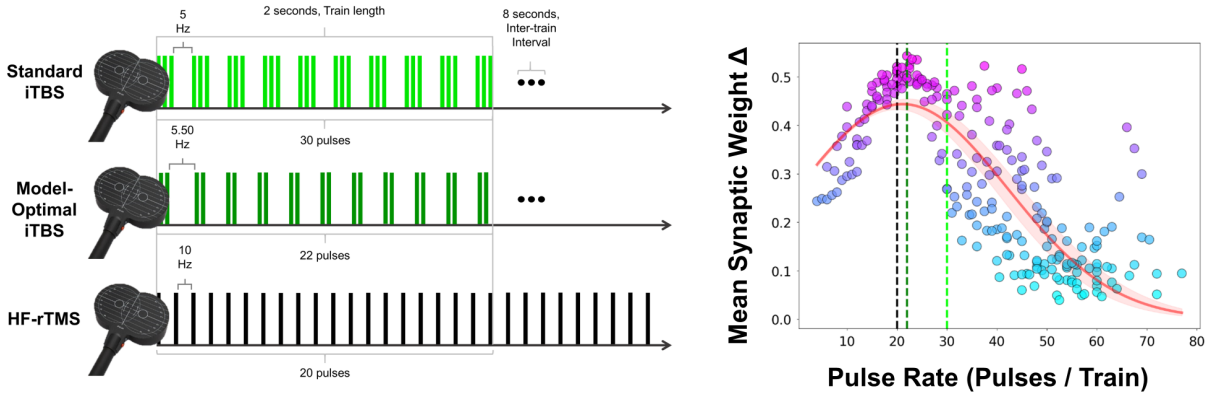

Figure S4: ***Illustration of circuit-mean synaptic weight change across pulse rate.*** Circuit-mean synaptic weight change over pulse rates, featuring canonical iTBS (lime), model-optimal iTBS (dark green), and HF-rTMS (black).

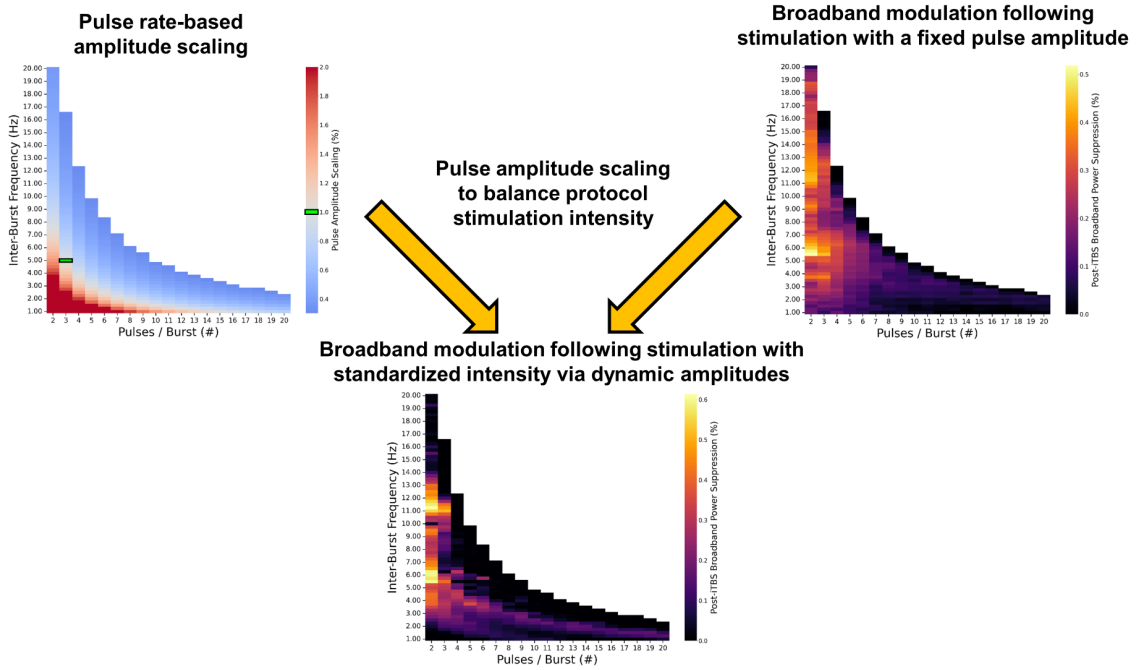

Figure S5: ***Method for standardizing protocol intensity.*** Scaling is based on the proportional stimulation intensity of canonical iTBS.

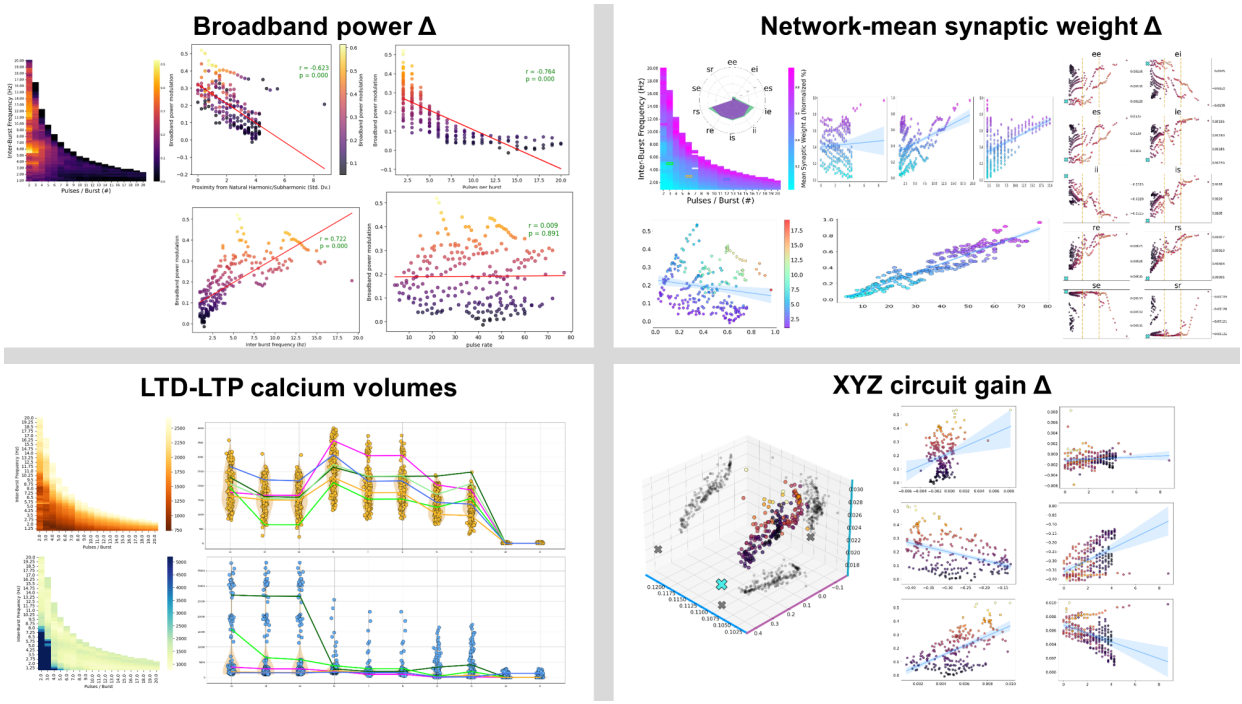

Figure S6: ***Primary analyses conducted with protocols using a fixed pulse amplitude.*** rTMS-induced effects on broadband power modulation, Circuit-mean and individual synaptic weight change, LTD and LTP calcium levels, and X, Y, and Z loop gains.

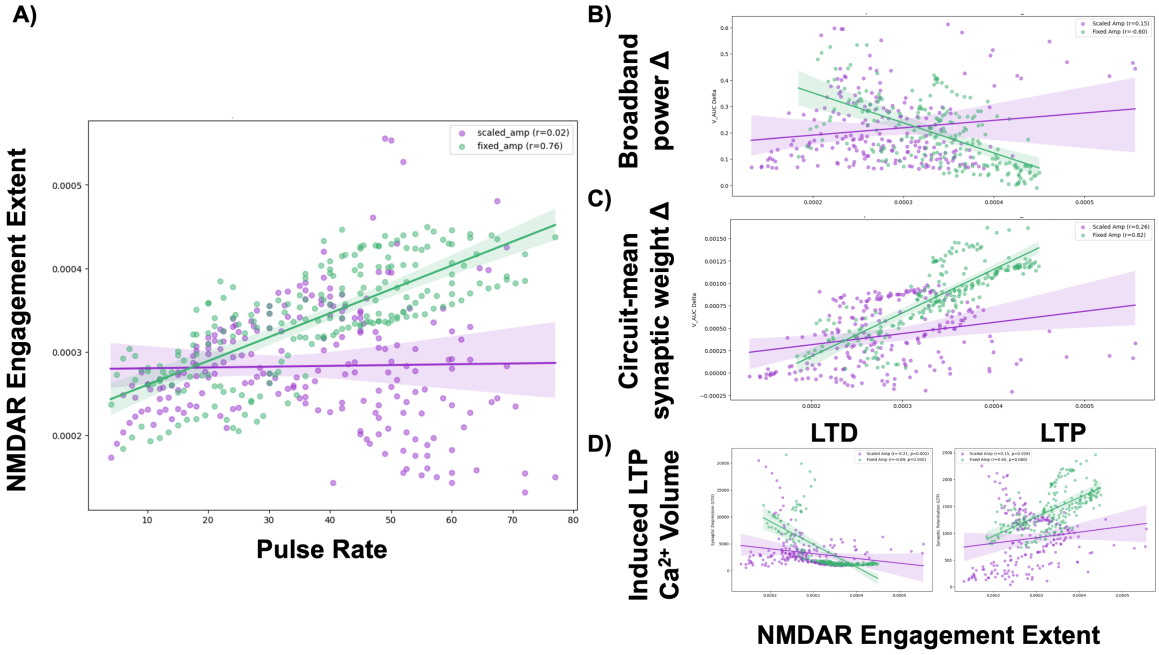

Figure S7: ***Comparison of active-stimulation NMDAR conductance variance between scaled- (purple) and fixed- (green) amplitude iTBS protocols.*** **A)** Relationship between protocol pulse rate and standard deviation of NMDAR conductance. Relationship between NMDAR engagement and **B)** broadband power modulation, **C)** circuit-mean synaptic weight change, and **D)** plasticity-inducing calcium volumes.